

Implementing and Investigating Refractoriness in LGMD Neural Networks

Mu Hua, HUA18720121

School of Computer Science

College of Science

A thesis submitted in partial fulfilment of the requirements of the University
of Lincoln for the degree of
MSc by Research

May 2021

Declaration

I hereby declare that except where specific reference is made to the work of others, the contents of this dissertation are original and have not been submitted in whole or in part for consideration for any other degree or qualification in this, or any other university. This dissertation is my own work and contains nothing which is the outcome of work done in collaboration with others, except as specified in the text and Acknowledgements. This dissertation contains fewer than 25,000 words including appendices, bibliography, footnotes, tables and equations and has fewer than 150 figures.

Mu Hua, HUA18720121

May 2021

Acknowledgements

My research was not and could not be finished by only me. Hence, now I would like to express my sincerest thanks to who had helped me in every aspect of my research.

First of all, I deeply appreciated my esteemed supervisor team, Prof. Shigang Yue, my primary supervisor who not only provided me with novel ideas of research directions but also offered me free-speak platform so that my ideas could come true step by step, and my second supervisor Dr. Wenting Duan who though is focused on another area of research, inspired me on thinking differently.

Secondly, in particular, I would like to thank one of my colleague Dr. Qinbing Fu for cherished time spent together in the lab, who guided me not only on experiments settings, data collection and analysis, but also computationally modelling and scientific thesis writing. Also, I would like to thank every colleague I have talked with, who offered to help me during my daily research life. Their works and ideas really expanded my vision and got me to know cutting-edge research topics.

Additionally and specially, my appreciation goes out to my parents, who have been and I believe will always be totally supportive, who encourages me to pursuit for the top of our knowledges, especially during such hard period of time. Their kind and infinite love has been my motivation to sail further.

Abstract

Collision can be threatening for animals including human beings. Thus, reliable and accurate collision perception is vital in plenty of aspects. Taking inspiration from nature, the computational methods of lobula giant movement detectors (LGMDs) identified in flying locust's visual pathways have positively demonstrated impacts on addressing this problem. However, collision perception methods based on visual cues are still challenged by several factors in physical world including ultra-fast approaching linear velocity and noisy signals. The current visual-cue-based LGMD neural networks could show ineffectiveness or generate false positive, especially when objects approach at fast velocity and when the video signals are polluted by noises. Hence, how ultra-fast approaching object in a colliding way can be detected remains to be further improved. Neural refractoriness, also known as refractory period (RP), a common mechanism inside animals' neural system studied for decades, though it has been considered to play a significant role in stabilising a neuron, has not been researched in the aforementioned LGMD neural networks for accurate and reliable collision perception. In this thesis, a novel method phenomenologically simulating neural refractoriness inside animals' neural systems is proposed and is further investigated on its functionality and efficacy when it is combined with the classic LGMD1 and LGMD2 neuronal networks for collision perception. Our systematically experimental results demonstrate that, mimicking refractoriness not only enhances the LGMD1 models in terms of reliability and stability when facing ultra-fast approaching objects, but also improves its performance against visual stimuli polluted by Gaussian or Salt & Pepper noise. Potential proof of LGMD2 neural

network's reliability and its capability to adapt to cluttered physical world is also provided. This research shows that, modelling of refractoriness can be effective and benefiting in collision perception neuronal networks, and be promising to address the aforementioned challenges for collision perception.

index: LGMD neural networks, collision perception, refractoriness, ultra-fast objects, noise signals.

Table of contents

1	Introduction	1
1.1	Objectives	3
1.2	Contributions	4
1.3	Thesis Outline	5
2	Related Works	7
2.1	Collision Perception Methods	7
2.1.1	Conventional Collision Perception Methods	7
2.1.2	Bio-inspired Neural Networks for Collision Perception	14
2.1.3	Sunmmmary	20
2.2	Neural Refractoriness	21
3	Methodology	25
3.1	Mimicking RP	26
3.1.1	pseudocode	27
3.2	LGMD1 neural network with RP	27
3.3	LGMD2 neural network with RP	33
3.3.1	Parameter settings	37
4	Experiments	39
4.1	Dataset	40

4.2	Experiment evaluation	43
4.2.1	RP in LGMD1 experimental evaluation	43
4.2.2	RP in LGMD2 experimental evaluation	48
5	Conclusion and future work	61
5.1	Conclusion	61
5.2	Future work	63
	References	65
	Appendix A Data sets	69
	Appendix B Performance Evaluation	71

Chapter 1

Introduction

Collision could cause severe damages for not only properties but also animals including flying insects and us human beings. Hence, accurate and reliable collision perception plays a fairly crucial role for most of the creatures, mechanical devices as well[33, 36, 45, 12]. Currently, there are excellent works utilizing sensors, together with conventional and complex methods such as expansion segmentation[5] for collision perception, which realise recognition for imminent collision at acceptable cost of time delay and high-priced equipment. There are also outstanding works based on visual cues which are crucial for insects to navigate, collision-free, utilizing normal cameras to conduct collision perception[8]. One of them is the lobula giant movement detectors (LGMDs), taking inspiration from flying locusts[44]. Benefiting from prolonged evolution, flying locusts have been provided with a vision system which shows positive effects on their evading behaviour and improves their success rate of escaping from their natural predators coming in the blink of an eye. Within this relatively short period of time, several sets of neurons, including the LGMD1 and LGMD2 neurons, which respond mainly and selectively to targets on a collision course, and the descending contralateral movement detectors (DCMDs) to pass neuronal spikes to trigger evasive glide, collaborate closely to achieve avoidance[29, 28, 34]. Upon these solid prior knowledges concluded by outstanding neuroscientists, LGMDs neural networks have been established

for quick collision perception. Compared to the conventional and integrating methods that require sensors such as LiDAR or radar, and high-computational-power GPU, the bio-plausible LGMDs neural networks, low in algorithm complexity, are able to respond to the approaching objects with less time delay at comparative success rate[20].

However, though LGMD1 and LGMD2 neural networks have respectively demonstrated positive impacts on addressing the collision perception problems, they could show ineffectiveness or generate false positive responses under certain circumstances, especially when (a) the approaching object is ultra-fast and (b) the signal is noise-polluted. Here, when 'ultra-fast' is brought up, the velocity of the objects up to 10 m/s , which is around 3 times the speed a desert locust can reach. Due to these two factors, current LGMD1 and LGMD2 neural networks become less stable and generate action potentials while there is no collision or the approaching object is still far away. Thus, how these LGMDs neural networks can be further improved and stabilised remains to be explored.

Neural refractoriness, known also as Refractory Period (RP) in both invertebrates' and vertebrates' neural system, is a common phenomenon[4, 17]. Caused by inactivation of sodium channels that help depolarize the membrane, one entire process of RP is divided into absolute refractory period (ARP) and relative refractory period (RRP) as shown in Fig. 2.17. Within the short period of time of ARP, neurons remain completely silent while during RRP, they retain the possibility of producing spikes again for stronger stimuli[18]. Though it is well acknowledged that refractoriness helps to keep a neuron stable by limiting its number of action potential, it has not been considered in the research of LGMDs neural networks for collision perception to further improve their robustness and reliability.

Therefore, in this thesis, a novel method phenomenologically simulating neural refractoriness is proposed, and subsequently applied to the previous works of classic LGMD1 and LGMD2 neural networks for collision perception to further investigate its feasibility, functionality and efficacy when the incoming object approaches at ultra-fast velocity and the

input signal is contaminated by either types of ‘Salt & Pepper’ noise or ‘Gaussian’ noise. The experimental results demonstrate that, mimicking refractoriness not only stabilises the LGMD1 models when the objects is approaching at ultra-fast velocity, but also improves its performance against visual stimuli signals polluted by Gaussian or Salt & Pepper noise. For LGMD2 neural networks, experimental results should provide potential proof of its reliability and capability to adapt to cluttered physical world. This research shows that, by numerically modelling of refractoriness, LGMDs collision perception neural networks is benefited and partly improved. Thus, modelling refractoriness can be promising to address the aforementioned collision perception challenges and it is its being simple in terms of computational complexity that make it possible to be further integrated with micro-robot such as Colias.

1.1 Objectives

The main objectives of this work include:

- To mathematically simulate the neural refractoriness mechanism by means of approaching its membrane potential change curve during refractory period in a simple method.
- To verify the feasibility of integrating proposed mechanism with both classic LGMD1 model, which generates most responses to the looming objects and the LGMD2 neural network, which prefers to produce spikes to dark incoming objects against brighter background.
- To further investigate the effects that the phenomenological neuronal self-silencing mechanism imposes on the LGMDs collision perception neuronal networks, especially the looming objects approaching at ultra-fast linear velocity.

- To further explore whether and to what extent, mathematical mimicking neural refractoriness helps to retain robustness, reliability and stability of LGMD-based collision perception neural networks when the input images are contaminated by noises, including Gaussian noise and Salt & Pepper noise.

1.2 Contributions

By addressing the listed objectives, this work results in the following contributions:

- Brief background research of conventional methods for recognizing collision that have been utilized on ground vehicles as well as on unmanned aerial vehicles. Introducing LGMD-based collision perception neural networks, comparing conventional methods for collision perception with the bio-inspired LGMD neural networks based on visual cues. Briefing neuroscientific principle of neural refractoriness together with modelling of refractoriness.
- A simplified method mimicking refractoriness and two proposed neural models (LGMD1 and LGMD2) with neural refractoriness mechanism.
- Datasets consisting of more than two hundred clips of a black ping pong ball colliding into the camera lens at various velocity, usually at the speed around 6 m/s , up to more than 9 m/s at the various sampling rates of up to 240 Hz .
- Thorough experimental evaluation of the two proposed neural networks and assessment of their functionality and efficacy for addressing current challenges that LGMD collision perception neural networks are facing.

1.3 Thesis Outline

The structure of the remaining is organised as follows: Chapter 2 reviews the most related works including three aspects: conventional collision perception methods, LGMD neural networks and modelling of refractoriness. Chapter 3 elucidates our proposed methods together with both LGMD1 and LGMD2 neural networks in detail. In the following Chapter 4, firstly the obtaining of datasets is introduced, secondly systematic experimental results are demonstrated. The last Chapter 5 concludes this research and describes future works.

Chapter 2

Related Works

In this chapter, most related works are reviewed and introduced. They are divided into two parts: 1) collision perception methods, including two sub-sections: a) conventional ones usually demanding multiple sensors coordination, and b) bio-inspired methods collision perception taking inspiration from crab, pigeon, fruit fly and locust, mainly LGMD1 and LGMD2 neural networks from locusts. In this part, visual cue-based collision perception methods are compared with the conventional ones in terms of cost, accuracy and their applications are also briefly introduced. Since this research is focused on what impacts neuronal refractoriness implements on previous works of LGMD neural networks for collision perception, the second part is 2) studies of refractoriness starting with its principle in biology and then mathematical modelling.

2.1 Collision Perception Methods

2.1.1 Conventional Collision Perception Methods

For the number of ground vehicles increases a great deal since their invention, traffic accidents come along resulting in not only unexpected casualties, but also huge property loss. Thus,

how these tragedies can be avoided has been a widely discussed topic that is related to our daily life. The detecting of objects on a colliding trajectory, as the step prior to avoidance behaviour, plays a crucial part. Currently, with economy and technology advancing in a magnificent manner, collision perception becomes a equally vital challenge for UAVs and human-robot interaction area such as factories where manipulators are operating.

In [1], a simple approach of collision perception was proposed based on measuring the distance between ego-vehicle and cars in front. By using a ultrasonic ranging device (URD) that sends out signals, the onboard processing device outputs the 'minimum safety distance' and if it becomes too small, the driver will be alerted to slow down to keep safe distance or the system will step in and temporarily take over the brake. This method works properly but the drawback is that it requires a sender and a receiver for ultra-sonic signal.

To address the real-world challenges, Baek et al. in [2] brought up a method, which made use of both vehicular communication as well as onboard sensors, such as Lidar, radar and camera. Combining all the key data transmitted from onboard devices and remote vehicles (RVs), future trajectories of the host vehicle (HV) and RVs can be predicted (Fig.2.1), so that alert is sent in time according to the estimated time-to-collision (TTC). They also pointed out that the vehicular communication can be further extended to vehicle-to-everything (V2X). More specially, not only surrounding vehicle-to-vehicle (V2V) communications, accurate vehicle-to-pedestrian (V2P) and vehicle-to-infrastructure (V2I) data exchanges also contribute to preventing collision from occurring in the future. The V2V or V2X strategy can be promising. However, the limitation of scheme like this requires more costly sensors, which result in the need of a high-performance CPU to run real-time calculation. Not to mention that methods based on multi-sensor fusion can be quite limited by several physical factors, i.e. occluding weather and the field-of-view (FOV) of the sensor.

Sun et al. also adapts the V2V communication in [38], proposing a novel rear-end collision perception as shown in Fig 2.2. Different from [2], their method is an integrated

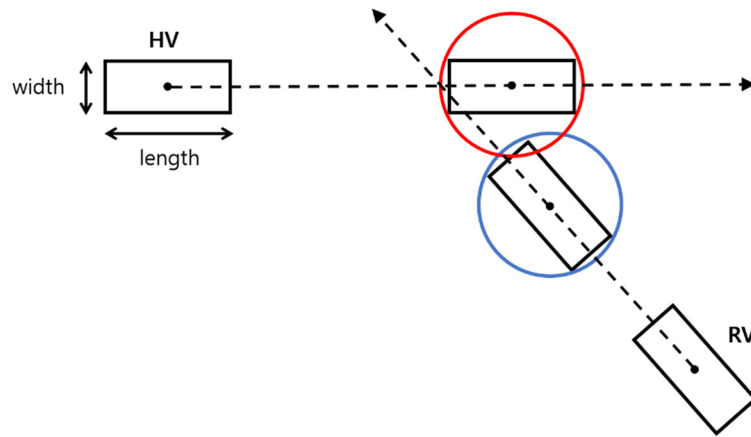


Fig. 2.1 Illustration for finding a possible collision event using the predicted trajectories of the host vehicle and the remote vehicle[2].

algorithm. Firstly though combining Global Navigation Satellite Systems (GNSS), electronic compass and lane segment information, each vehicle can be high-precisely real-time located. Positioning information is then passed to a Cubature Kalman Filter (CKF) to calculate relative information such as relative distance (RD), relative velocity (RV) and relative heading (RH). Subsequently, the adaptive neurofuzzy inference system (ANFIS), which has been trained, judges the status of the following car. One of the advantages of their method is that the whether matters little, and after training, the decision making system can be robust. However, their system could be blind when the road lanes are blurry and the GNSS signal is weak.

Beside above methods that requires data exchange between two vehicles, there is one method proposed by Nedevschi et al. utilizing sensors and stereo vision to realise forward collision perception locally and independently[23]. The proposed method exploits a dense stereo system and onboard sensors to extract and abstract obstacles in the real-time real-world driving scenario (elevation map) in a 3D manner. According to mechanical parameters and yaw rate et al. of the ego-car, a drivable tunnel is calculated and described by a polyhedron (see Fig.2.3 from [23]).

For UAVs, it's quite vital to accurately recognize obstacles in case of crashing. One way is to use optical flow method based on gradient method of Lukas-Kanade to extract depth

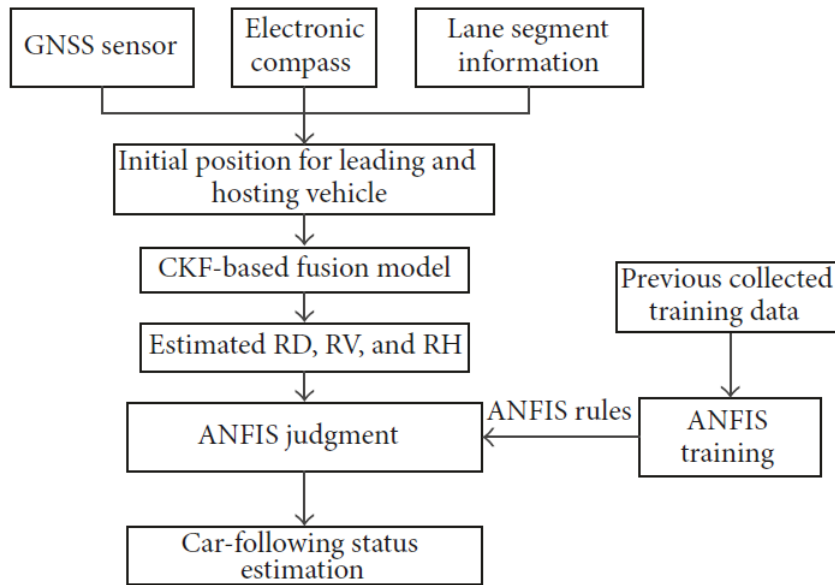


Fig. 2.2 The proposed novel rear-end collision detection system overview. The combined system firstly gathers precise positioning information from GNSS. Subsequently together with e-compass and traffic lane segment information, relative positioning between two user vehicles can be obtained through CKF-based fusion model. After that, the pre-trained ANFIS judgement estimate the following status between two user vehicles to decide whether there is rear-end collision. [38]

information from images captured by a onboard camera[16]. The possible obstacles are located by selecting optical flow vectors which are extended though the heart of the image and in the meanwhile 20 pixels away from it (see Fig.2.4a). Then the length of these vectors are used to estimated the distance between ego-vehicle and the potential obstacle so that depth information can be obtained (Fig.2.4c).

In [3], Bareiss et al. proposed a feed-forward method. Based on integrated information provided by the pilot input and onboard sensors, the UAV is able to continually extrapolate the initial trajectory. Subsequently, uncertainties in the real-world such as sensing and estimating uncertainties are taken into account within its collision avoidance algorithm to estimate a change in the initially input pathway. This way, the UAV is capable to conduct collision

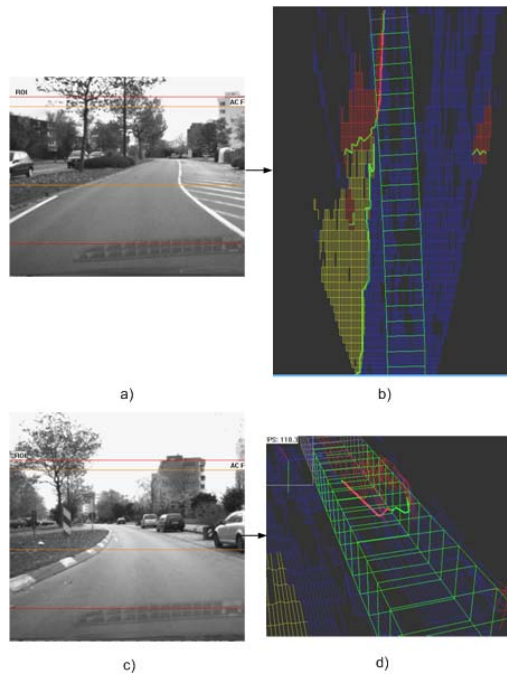


Fig. 2.3 a) and c) is the left and right image captured by the dense stereo system respectively. b) describes the top view of the 3D elevation map, whilst d) is the free look perspective. The blue area represents drivable points; yellow area show curb points; red points are detected object points; the green polyhedron (green rectangles in sub-figure b) elucidates the drivable tunnel.

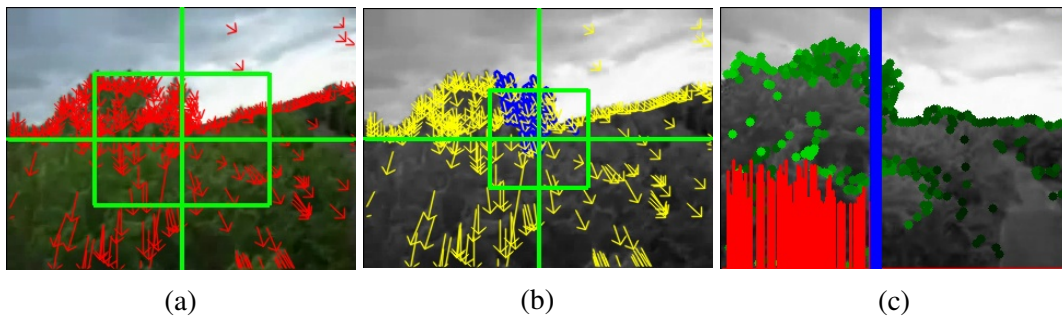


Fig. 2.4 (a) Optical flow vectors. (b) The potential dangerous area is described by blue points. (c) Evaluation of distance from the obstacle. Depth information can be extracted from the discrimination of the distance, which is represented by different shade of green colour. This image is adapted from [16]

perception and figures out a safe way with a probability within selected confidence bound, even the pilot deliberately attempting to crash the vehicle.

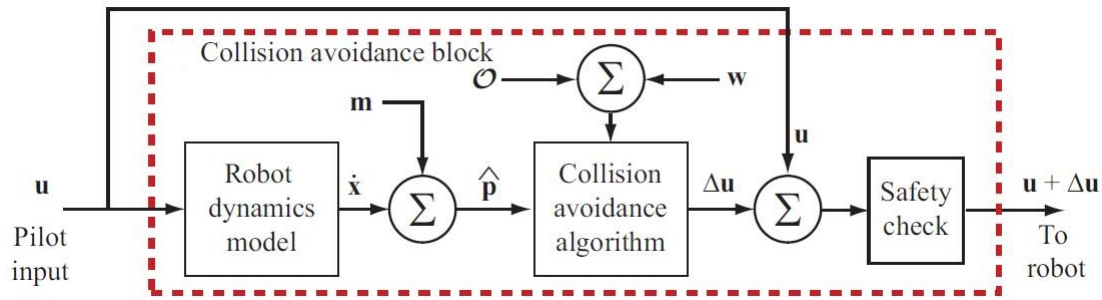


Fig. 2.5 Control block diagram, where u , pilot's commands, is injected together with the motion model uncertainty m into the dynamic model to obtain the initial path, p . The path, together with uncertainty w , is checked against obstacle O . If collision is possible, a change (Δu) of the initial pilot input is calculated. Final safety check makes sure that the UAVs moves collision-free. Inside the red dash-line rectangle is the collision avoidance decision making system algorithm. This image is adapted from [3]

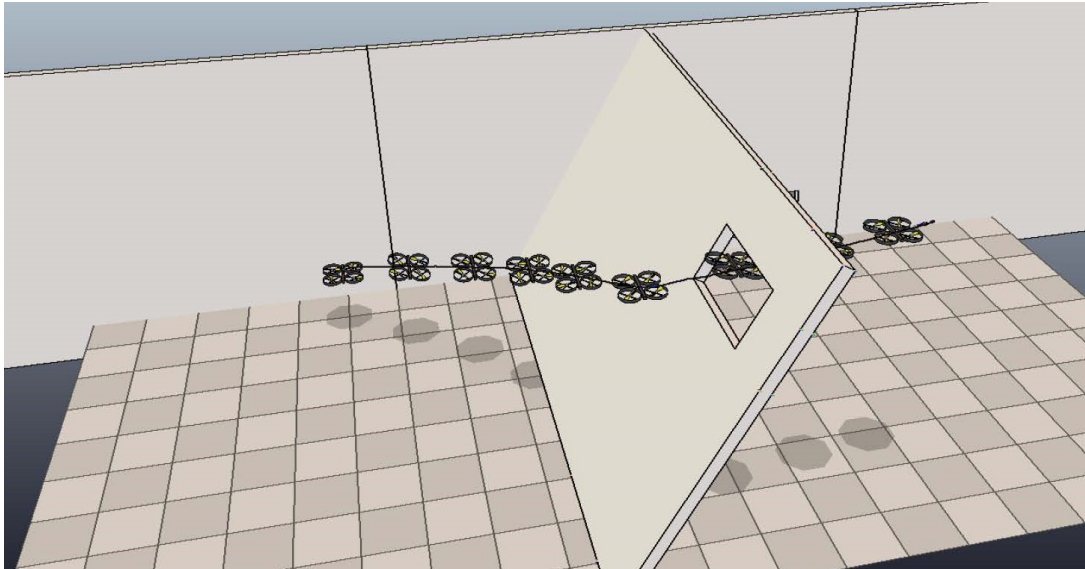


Fig. 2.6 3-dimensional example is shown where the quadrotor is steered towards a goal point through a window on a slanted wall, image adapted from [3]. The window has tight clearance with respect to the robot. The height of the window is only 25% larger than the robot's diameter, however, the diameter is a conservative estimate provided by the minimum-radius bounding sphere. The width of the window is 75% larger than the robot's diameter.

Apart from the low altitude obstacles, another sort of accidents that UAVs are involved from time to time is conflict with other unmanned aerial systems (UAS) and even airliners. To make UAVs coexist safely and effectively with current manned aeroplanes, Zsedrovits et al proposed a effective method to detect intruder aircraft from up to 1km away with the

around 1m accuracy[48] (Fig.2.7). This image-processing-based algorithm works properly with constraints such as electronic power and wireless communication, whilst needs more information when the contrast of the cloud is not too high.

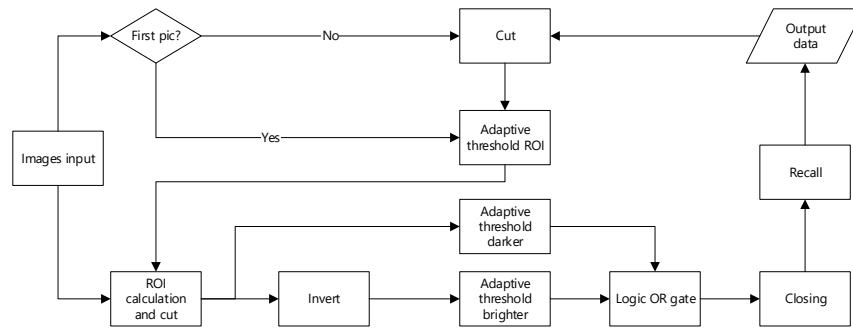


Fig. 2.7 Schematic of the proposed method. The first step is to filter out slow transitions in the input images, and adaptively fix the ROI together with data from last moments. The following step is to result a binary image, containing brighter and darker image of the detected aeroplanes, after gray-scale processing and cutting the image within the ROI, which shall be then combined with the binary image from last moment for more accurate aeroplane extracting.

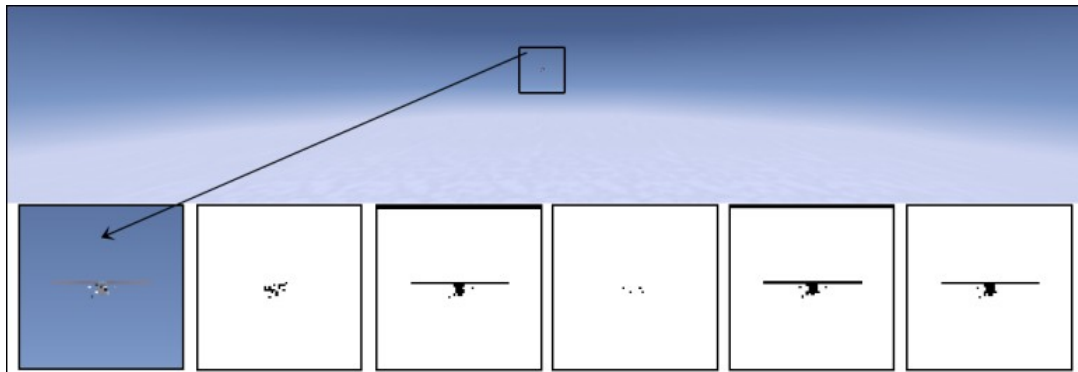


Fig. 2.8 Steps of the proposed method. Top is the input image. Bottom shows outputs of every step, from left to right respectively: the coloured region of interest (ROI), adaptive threshold, darker pixels, brighter pixels, logical OR gate and closing, segmented aircraft[48]

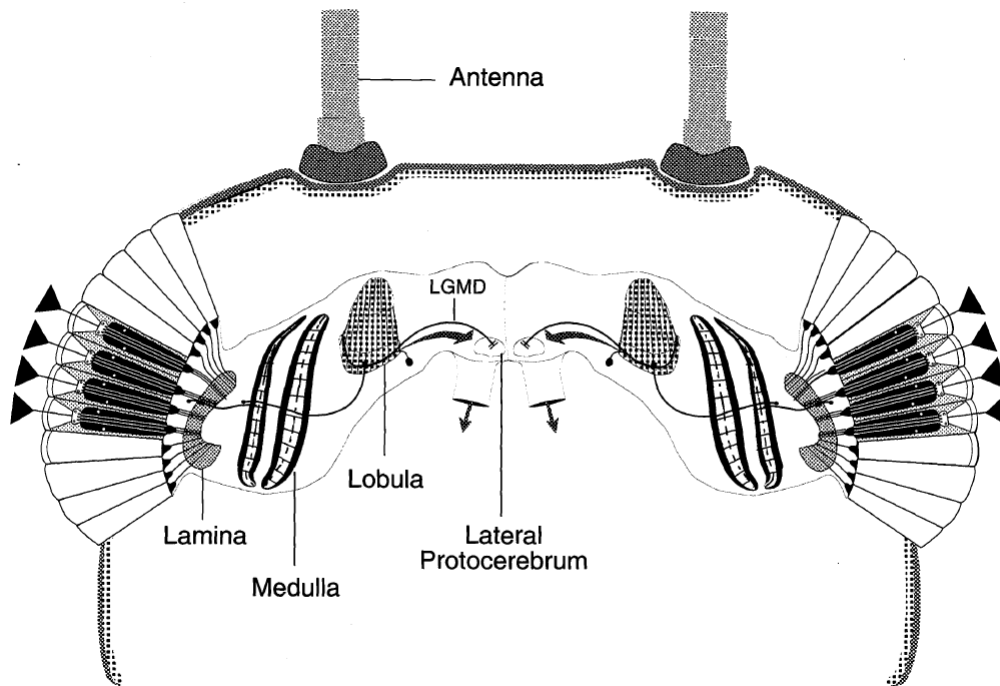


Fig. 2.9 Schematic drawing of a horizontal section through the locust head to show organisation of the visual system and the LGMD/DCMD pathway from [26].

2.1.2 Bio-inspired Neural Networks for Collision Perception

Thanks to millions of years evolution, invertebrates have been provided with reliable and robust visual systems that allow them to survive cluttered environments and predating enemies coming out of nowhere at surprisingly high speed. Inside certain species' visual neural pathways, such as crabs', pigeons', fruit flies' (*drosophila*) and desert locusts', collision perception neurons play a relatively critical role[14, 37, 7, 25, 6, 22]. Taking locusts' as a typical example, LGMD for its distinct features is widely researched for collision perception, together with descending contralateral movement detector (DCMD) to escape from impending collision.

LGMD1(?), identified in the lobula layer inside its visual pathways, has firstly been discovered as movement detectors in [24], then been recognized to produce the most frequent spikes to objects on an approaching course while respond weakly to receding or translating

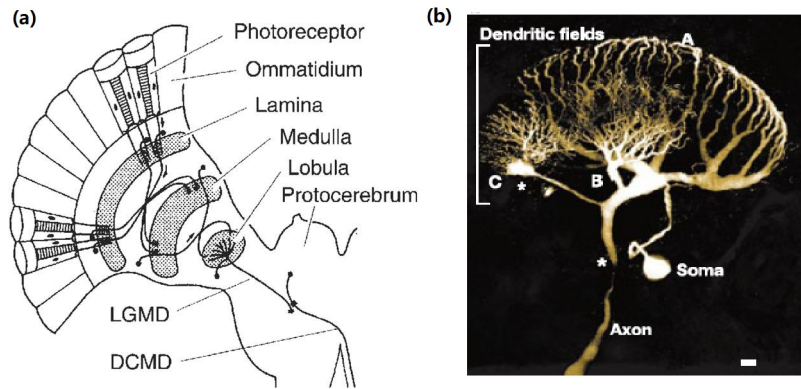


Fig. 2.10 Illustrations of the LGMD1 morphology: (a) Presynaptic neuropile layers of the LGMD1 neuron and the postsynaptic one-to-one target DCMD neuron, adapted from [29], (b) LGMD1's large dendritic fan (A) and two additional dendritic fields (B, C) that receive distinct synaptic inputs, adapted from [15]

objects[30]. Subsequently a neural network composed of four layers of neurons as shown in Fig.2.11, namely the photoreceptor layer (*P* layer), the excitation layer (*E* layer), the inhibition layer (*I* layer) and the summation layer (*S* layer), was proposed by Rind together with Bramwell [27], based on which mathematically modelling of the LGMD1 was further accomplished by Gabbiani et al. focused on angular velocity in[15].Based on the structure shown in Fig. 2.11, Yue et al. in [45] by adding a novel group layer (*G* layer, as shown in Fig. 2.12), which concluded, through offline and online experiments, that the classic LGMD model equipped the mini-robot, Khepera robot (K-Team, Switzerland) at the speed of 32 *mm/s*, with the ability of cruising autonomously and free of collision in real time inside the experimental arena. The model was then similarly converted to an embedded visual system strategy. Hu et al. applied this method to a micro-robot, proving its high precision and reliability in collision perception by running the micro-robot at various velocities from 1.5 *cm/s* up to 17 *cm/s* in a arena with several sets of densities of obstacles[20]. Recently, by choosing a larger convolutional mask, Zhao et al. expanded LGMD1 model's application field to small quadcoptors, equipping them with ability of sensing impending collision[47]. To enhance the precision and expand the application of visual-based collision perception

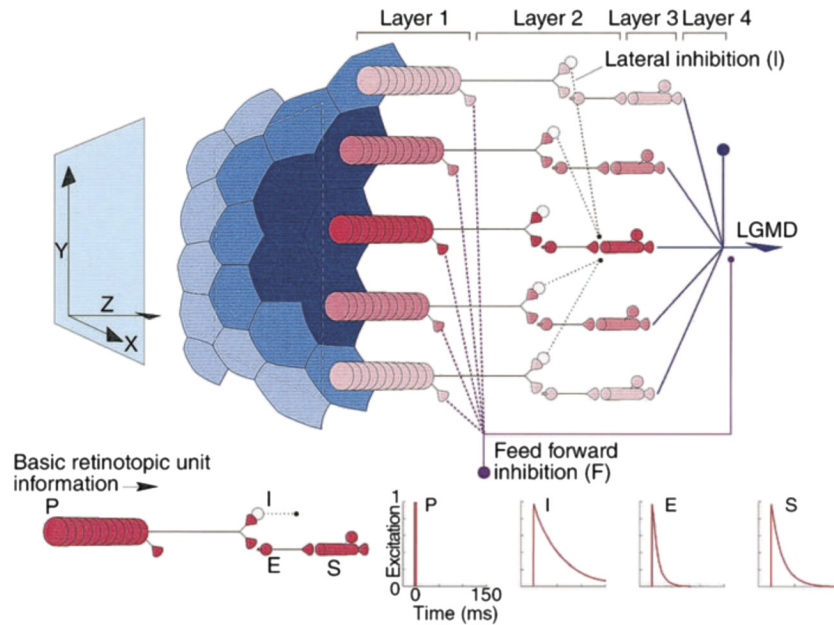


Fig. 2.11 Schematic representation of the neural network LGMD adapted from [29]. The inputs to the network were a series of computer-generated images of a moving object. The input organization of the basic retinotopic unit of the network is shown in red and labelled. The ‘P’ cells, corresponding to the ‘Layer 1’, receive direct luminance changes from environments and pass them to next layer, where ‘E’ cells are instantly excited and ‘I’ cells are excited with one moment delay. The excitation and inhibition information from ‘E’ and ‘I’ cells is then summarised in ‘S’ cells in ‘Layer 3’. The ‘Layer 4’ then accumulates output of all ‘S’ cells.

neural networks, an integrated model of LGMD1 and translating sensitive neural network (TSNN), which consists of four directionally sensitive neurons based correlated elementary movement detectors (EMDs), was proposed by Yue et al. in [46]. Additionally, a specialized decision-making mechanism coordinates with the integrated model, achieving more reliable and robust responses to cluttered background.

As an interneuron of LGMD1, LGMD2, though shares the same features of responding more strongly to looming objects, has its distinct characterization. Having been found to mature early in juvenile locusts, this group of neurons has been investigated to show most preference to dark incoming objects within a bright background, which resembles their surviving environment as young individuals, than a dark background[40]. Regardless of its significance for locusts that mainly live on the ground, only a few studies have been

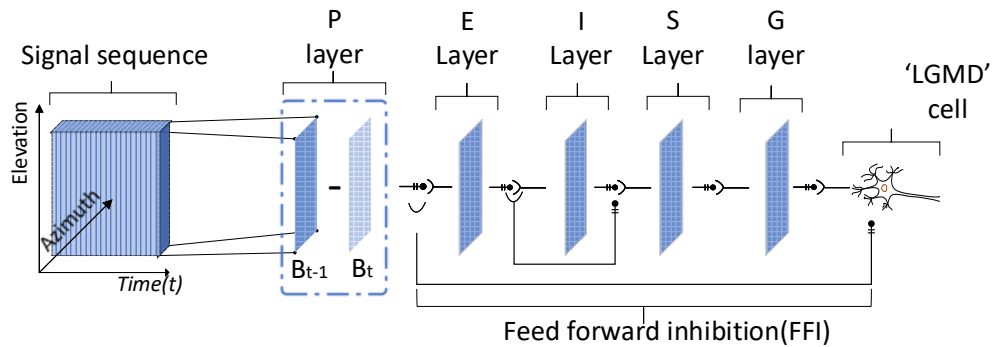


Fig. 2.12 Schematic illustration of the LGMD-based neural network for collision perception. There are five layers and two single cells: Photoreceptor layer (P); excitatory and inhibitory layer (E and I); summing layer (S); grouping layer (G); the LGMD cell; and the feed forward inhibition cell (FFI). The input of the P layer is the luminance change. Excitation is indicated right after P layer, accepts output of P layer with no delay. Lateral inhibition is indicated after E layer receive E output with one frame delay. The FFI also has one frame delay. The input to FFI is luminance change information from photoreceptor layer.

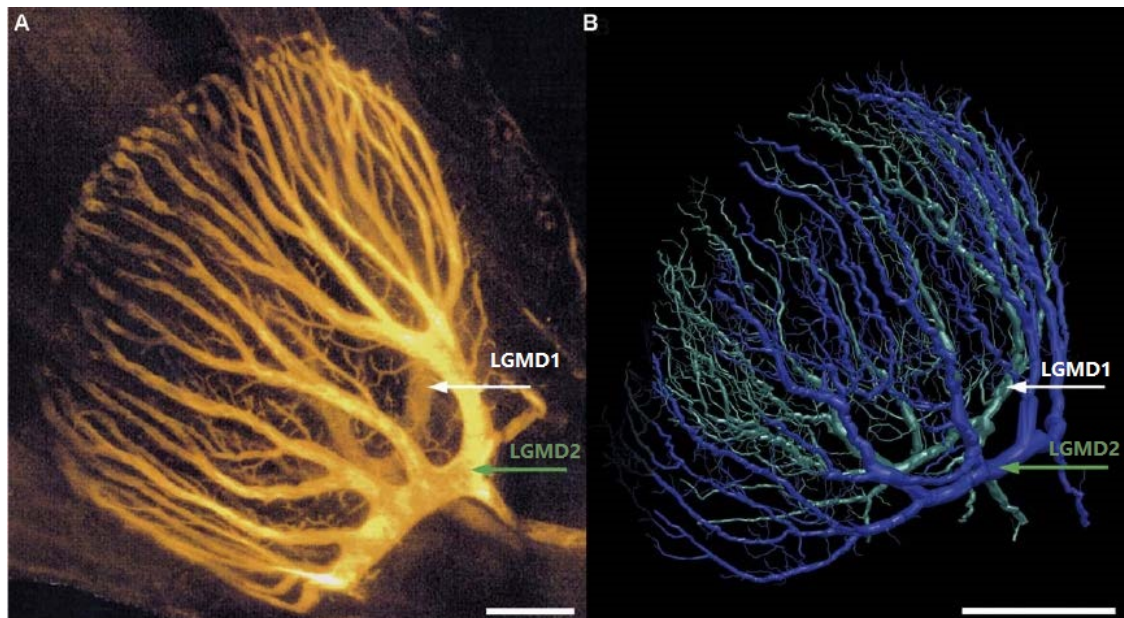


Fig. 2.13 Validity of the reconstruction method. Comparison between a confocal reconstruction of the two LGMD neurons stained intracellularly in an adult (A) and a Bodian based Neurolucida reconstruction of the same neurons in a 5th instar (B). White arrows point to the LGMD1 and green arrows to the LGMD2. This image is adapted from [39].

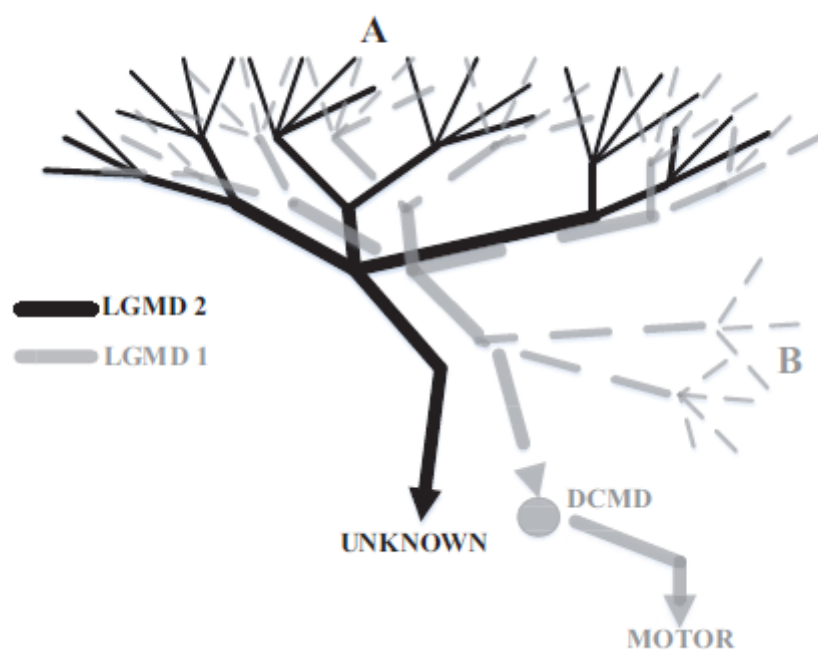


Fig. 2.14 Schematic diagram of the LGMDs morphology. Sub-field A indicates the pre-synaptic dendritic structures of both LGMDs. Sub-field B indicates the FFI pathway of LGMD1 which is absent from LGMD2 [12]. DCMD is a one-to-one post-synaptic target neuron to LGMD1 conveying neural signals to motor; the partner neuron of LGMD2 remains unknown [12], [15]. This image is adapted from [11].

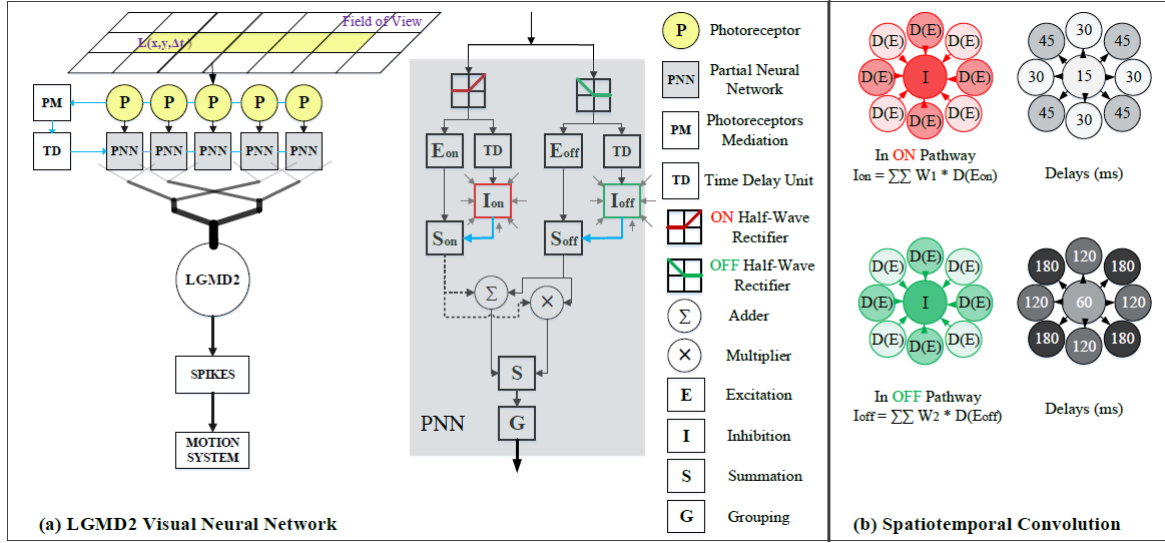


Fig. 2.15 Schematic of the LGMD2 visual neural network (a) and spatiotemporal convolution (b). Note that five photoreceptors are selected just for example. Each P cell connects to the PNN, namely the ON & OFF channels followed by the S layer and G layer. Two blue lines represents the photoreceptor mediation (PM) mechanism pathway. This image is adapted from [11].

published. It is only after 2015 that computationally modelling of LGMD2 was completed by Fu and Yue[13], realising its selectivity to light-to-dark luminance changing by introducing a novel mechanism of ON & OFF parallel channels as shown in the ig. 2.15, discriminating luminance increment and decrement. More specifically, in the ON channels, which are rigorously sieved, inhibitions and temporally delayed excitations are produced while in the OFF channels, direct excitation and temporally delayed inhibition are generated[10]. Both offline tests and real-time experiments on the aforementioned micro-robot demonstrated feasibility and robustness of this creative algorithm[11].

There are also excellent bio-inspired works for collision perception taking inspiration from crabs, pigeons and fruit flies. In [25], the monostratified lobula giant neurons of type 1 (MLG1) has been modelled in a way similar to LGMD neuron in locst, then verified and realised its biological features to peak when an approaching object on a collision course reaches a fixed threshold at degree of 49 and to respond at the beginning of approach. This

work is then improved by Carbone et al. in [6], with angular speed and its relation with information delay considered, realising multiple neuronal responses to luminance change, rotational and translational optical flow. In the pigeon nucleus rotundus, three neurons have been identified to be responsible for the calculation of approaching objects, two of which is sensitive to absolute and relative image expansion rate, the remaining to another optical variable. Focused on angular image expansion rate, this work is modelled based on several partial differential equations and linear calculation, managing to be elicited by looming isolated objects. Different from LGMD neural networks, the modelling for looming sensitive neurons in crabs and pigeons has been focused on the angular velocity and size and image expansion rate, while the LGMD neuron networks are only edge expansion sensitive, despite of its linear or angular speed.

2.1.3 Summary

Those conventional methods for collision perception that has been applied to ground vehicles and UAVs, are distinguished by their accuracy and reliable in certain scenarios. However, considering the sensors such as LiDAR, radar, the hardware required such as high-performance computing and image processing unit and RGBd camera and special devices to receive GNSS positioning information, it can be fairly costly on the one hand, and large in size on the other hand. Thus it is more suitable for devices or machines that are spacious for multiple hardware fusion, and tough to be integrated with micro-robot platform such as Colias.

The LGMD-based visual cues processing algorithms, on the contrary, are showing advantages such as being low in algorithm complexity while proved high in success rate and being affordable for requiring only normal RGB camera. Therefore, the LGMD bio-inspired neural networks perform better in terms of balancing costs and success rate, demonstrating much higher possibility to be applied onto micro-robot platform.

Though the aforementioned LGMD models have made remarkable contributions to collision perception systems based on visual cues and in turn inspired exploration on coordination mechanism of interneurons, their performance could become unstable and drop sharply under certain circumstances, such as the velocity of an object on a colliding trajectory is relatively high, up to 9.6 m/s and the input signal (image) is noise-contaminated. Since it takes input from solo RGB camera, it also shows ineffectiveness while the environment is poor in light condition. Besides, neural refractoriness, as a common neuronal behaviour to help maintain stability of a single neuron, has not been considered and simply mathematically described in previous modelling works.

2.2 Neural Refractoriness

Refractoriness has been comprehensively noticed and investigated as a spontaneous mechanism inside animal neural systems for a considerably long time. It occurs and comes after an action potential is produced. The process of depolarization opens sodium ion (Na^+) channel in the meanwhile slows down the activation of potassium ion (K^+) channels and Na^+ channel inactivation, resulting in the process of repolarization of the membrane potential as the action potential sweeps along the length of an axon (see Fig 2.16). Following the action potential, Na^+ channel becomes inactivated while K^+ channel are activated due to concentration gradients for a brief time, during which it's harder for the axon to fire another spike. This spontaneous neuron self-silencing mechanism is called refractoriness. Thus, the refractory period limits the number of action potentials that a given nerve cell can produce per unit time. As might be expected, different types of neurons have different maximum rates of action potential firing due to different types and densities of ion channels. The refractoriness of the membrane in the wake of the action potential explains why action potentials do not propagate back toward the point of their initiation as they travel along an axon[17]. The approximated curve is shown in Fig. 2.17.

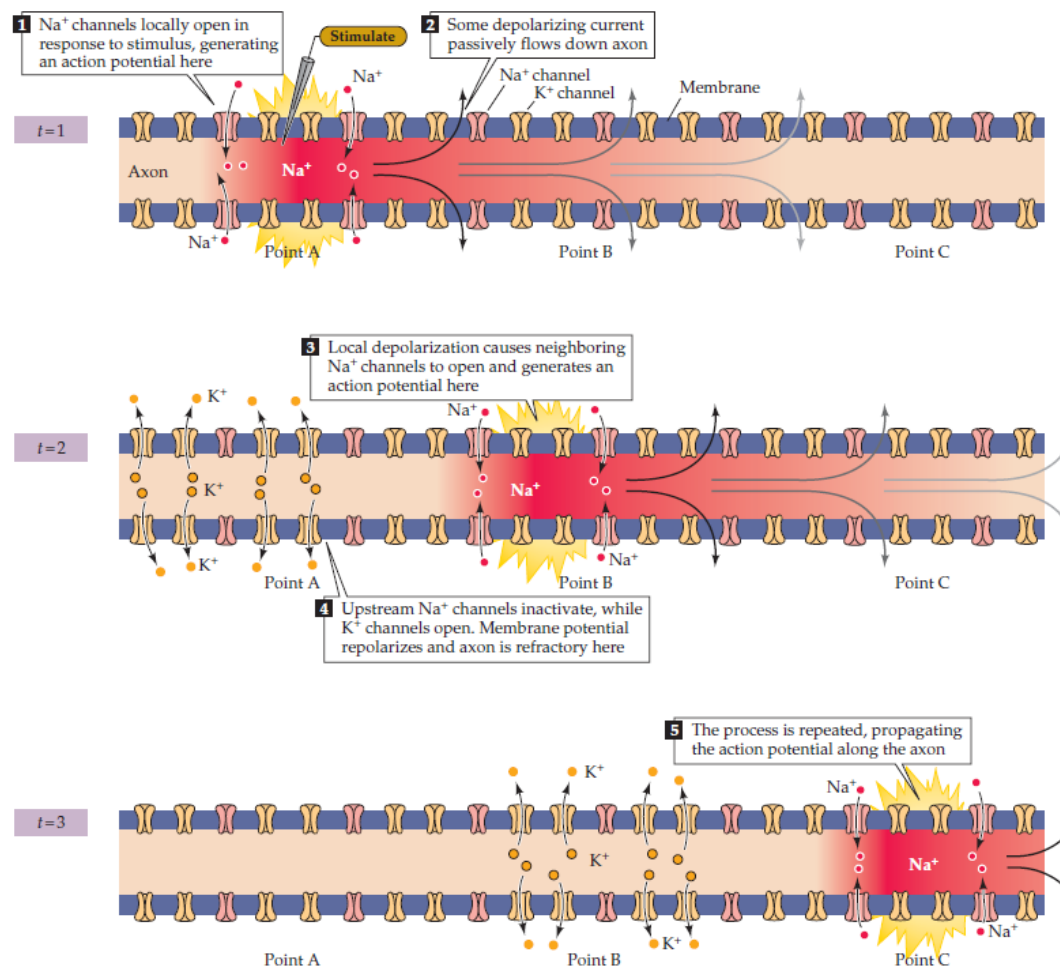


Fig. 2.16 One action potential travels along the axon from [17]. At Point A, the stimulus is applied to and Na^+ moves rapidly from outside to inside, resulting in depolarization in Fig. 2.17, where potential inside the neuron increase sharply, much higher than the outside until an action potential. In this stage, Point A shall not respond to any stimuli however strong they are. Then due to concentration gradient, K^+ flows towards outside the membrane, resulting in membrane potential drop sharp quickly, until reach the minimum, after which two types of cations start to move in and out slower to return to the resting state, as shown in Fig. 2.17, the process of Hyperpolarization.

Since the true values of membrane potential, such as the one of resting state, action potential peak vary from species to species, and even are different between two parts of body due to the sum of ions, it is hard to be described numerically accurate as a universal model.

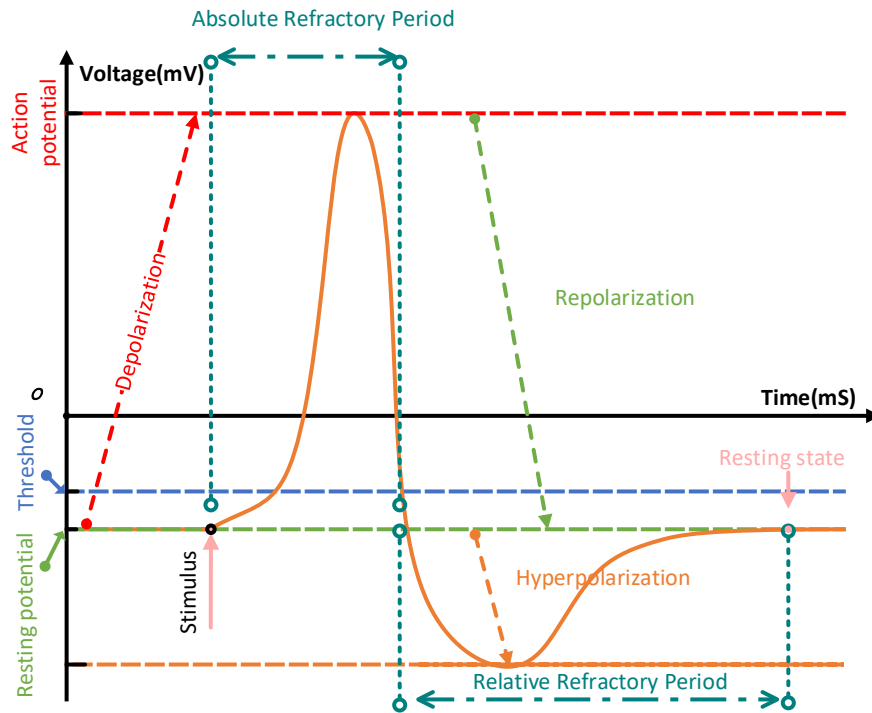


Fig. 2.17 One example of membrane potential approximate curve (in orange) of one neuron cell within the process of neural refractoriness. As a general property within all kinds of neurons, the whole process can be divided into two consecutive stage, namely 1) the absolute refractory period (ARP, between cyan dashed lines), which corresponds to the process of depolarization and a little proportion of repolarization and 2) relative refractory period (RRP, between cyan dashed lines), which is covered by hyperpolarization. Changes of membrane potential during depolarization and repolarization are respectively represented by red and light green dashed line with arrow. Similar monochromatic curve can be found in [17]. The thesis author owns originality of the very Fig 2.17.

For describing the change of membrane potential curve illustrated in this figure as accurately as possible, mathematically modelling of RP has been researched for decades. As far back as 1970s, Ruzi introduced ARP into a model of RATEN, random-threshold neuron-like element networks proposed by Amari, to further improve its stability in [31], presenting positive impact of integrating ARP with existing models.

As an issue of concern, after abundant efforts, mathematically modelling has made extraordinary progresses. In the attempts to reveal the code of information transmission between spiking neurons, several sorts of stochastic processes have been included to estimate

refractoriness[19]. In [21], a simplified Poisson process, which is utilized to estimate the characteristics of refractoriness is further adopted to suit other input inter-pulse intervals (IPIs). Ferrari et al. also proposed a method, which accurately reproduces the variability observed from ganglion cells of rat retina with correction to the Poisson process[9]. Another study from Schaette et al. proposed a renewal process with a recovery function to describe neural refractoriness. Though comparative experiments, this estimation shows close match between the observed locust auditory receptor neurons spike trains, presenting the significance of refractoriness to artificial neural networks[32]. Though Song et al. touched the combination of refractoriness and flies' photoreceptor, and elucidated what role RP plays in the encoding of graded neural responses, exploiting it for collision perception has not been considered[35].

By building computational models of RP, these works numerically contributed to our understanding the how underlying neuron circuits incorporate and the mechanism of how non-linear calculation conducts inside the neuronal pathways. However, it may be due to complexity in algorithm, infrequently are they considered to be integrated with collision perception visual models to further improve their accuracy and robustness, not to mention to be considered to be applied to micro-robot platforms, which are relatively low in computation power.

Chapter 3

Methodology

In this chapter, firstly, the proposed simplified modelling for neural refractoriness has been introduced, Secondly, 1) formulation of the proposed RP together with LGMD1 neural network, which consists four layers, Photoreceptor layer (P layer) accepts luminance changes, Excitation (E) and Inhibition (I) layer receiving outputs from P layer directly and with one frame delay respectively, Summation layer (S) summarising E and I outcomes in order to subsequently pass it to the LGMD neuron to be eventually calculated, is introduced. The proposed numerical mimicking RP model is inserted into LGMD1 model right after the P layer as a new layer called Link layer, ' L layer'; 2) formulation of the proposed RP with LGMD2 neural network, which has similar structure with a special ON/OFF channel for realising its selectivity to dark objects is shown. To endow LGMD2 with RP, neural refractoriness, the L layer is placed the same position as the LGMD1 model so that if one photoreceptor is activated, it steps into the ARP period, when it shall not respond again at all. Following one frame ARP, RRP, when it shall only be excited by stronger stimuli, lasts T_{decay} frames until the photoreceptor returns to its resting state.

The codes for the proposed RP model, and the LGMD neural networks endowed with neural refractoriness has been written in MATLAB and the outcomes of offline experiments,

the normalised potential values, are saved as '.mat' files, then plotted using a original MATLAB script.

3.1 Mimicking RP

Different from aforementioned mathematical modelling of refractoriness based on renewal processes to approximate the membrane curve, the goal of this proposed RP algorithm is to balance approximation and computational complexity in order to integrated on low-computational-power platforms. Hence, this proposed method mimicking neural refractory period is realised through adding a new layer called 'Link layer' (L layer), which consists of time-varying local threshold. The dynamic local threshold steps in when an already excited photoreceptor receives a subsequent stimulus to protect it from being wrongly and repeatedly activated, and to silence and hold the excited cell more stable, especially those non-lasting noises occur. Thus, only stimuli that are strong enough and lasting in time at the same time can be received by the excited photoreceptor and used by following layers to extract accurate edge expansion information. This way, at the cost of being a bit lower in terms of the normalised potential, the neuron generates accurate spikes when it is supposed to. More specifically, while the local thresholds can only be augmented by larger output, it shrinks over time as the following equation:

$$L_t(x, y) = L_{max} \cdot \alpha \cdot (1 + e^{i_t(x, y)})^{-1} \quad (3.1)$$

where $L_t(x, y)$ represents the local threshold at position (x, y) at the moment t , L_{max} defines the maximum of the local threshold. α is a scalar, whereas i is a naturally decay step factor,

calculated by:

$$i_t = \begin{cases} 1, & \text{if } P_t(x,y) > L_{t-1}(x,y) \text{ or} \\ & i_{t-1} \geq T_{decay} \\ i_{t-1} + 1, & \text{otherwise} \end{cases} \quad (3.2)$$

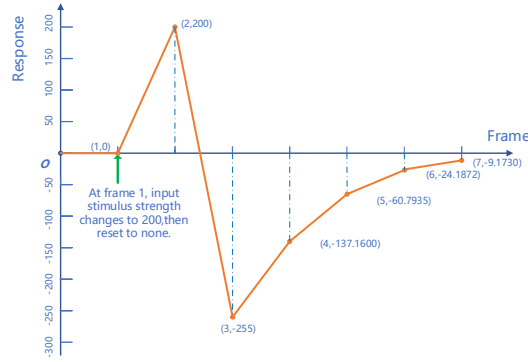


Fig. 3.1 The dynamic local threshold works as a filter to filter out stimuli weaker in order to protect the cell from being wrongly activated when still in the period of ARP or RRP. The orange curve show the change of $P_t(x,y) - L_t(x,y)$ when a single stimulus is applied at the 1st frame, which resembles the real membrane potential curve during refractory period. Since the aim of the proposed RP is designed to deal with discrete signals and the final membrane potential of LGMD neurons are normalised to $[0.5,1]$ to provide solution to an engineer problem, the membrane potential here is specific, unlike the one that can be measured in an actual locust.

3.1.1 pseudocode

3.2 LGMD1 neural network with RP

In this section, the strategy of the proposed RP mechanism fused with LGMD1 model is presented with formulations as well as parameter settings.

Sharing most structures of classic LGMD neural network in [45], the first layer, P layer of our proposed model is composed photoreceptors that are sensitive to brightness changing,

Algorithm 1 Pseudocode of neuronal refractoriness for single cell

```

1: threshold_L_origin = 0;
2: threshold_L_current = 0;
3: count_decay_step = 1;
4: tag_collision = 0;
5: for each frame ∈ [1, amountFrame] do
6:   if output_P > threshold_L_current then
7:     output_L = output_P;
8:     threshold_L_current =  $L_{max}$ ;
9:     count_decay_step = 1;
10:    tag_collision = 1;
11:   else
12:     output_L = 0;
13:     if tag_collision == 1 then
14:       threshold_L_current = threshold_L_origin +  $L_{max} * \alpha_{RP} * (1 + \exp(\text{count\_decay\_step}))^{-1}$ ;
15:       count_decay_step += 1;
16:       if count_decay_step >  $T_{decay}$  then
17:         count_decay_step = 1;
18:         tag_collision = 0;
19:         threshold_L_current = threshold_L_origin;
20:       end if
21:     else
22:       threshold_L_current = threshold_L_origin;
23:     end if
24:   end if
25: end for

```

and it is calculated by

$$P_t(x, y) = B_t(x, y) - B_{t-1}(x, y) \quad (3.3)$$

where $B_t(x, y)$ and $B_{t-1}(x, y)$ respectively corresponds to the luminance value of pixel (x, y) at the moment t and $t - 1$. The core of our proposed model lays in the L layer, which is placed between P and E layer to determine whether the output of P layer can be passed to its connected E layer. L layer, a 2-D matrix of the size of P layer, consists of local thresholds,

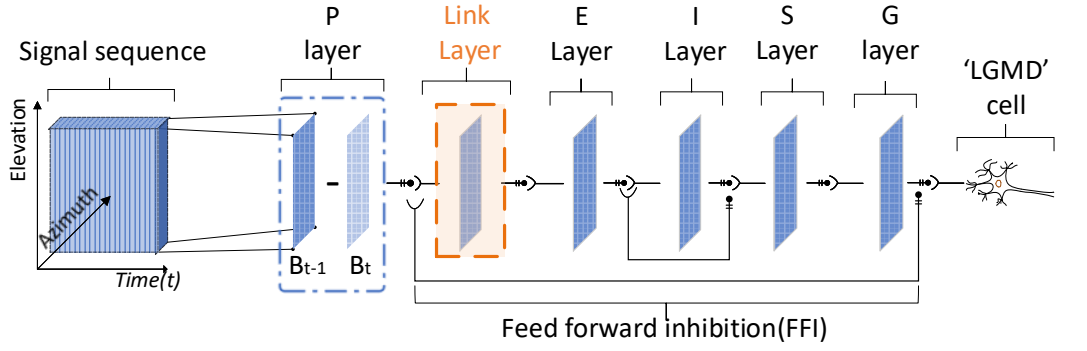


Fig. 3.2 Schematic of LGMD1 neural network with the Link layer. The blue cuboid on the left side represents motion stimuli. Within P layer, image frame at t time subtracts its previous one. The output of P is then conveyed to L layer, and so on.

and is defined by both a decay indicator i_t and the value of corresponding P layer cell:

$$L_t(x, y) = \begin{cases} L_{max}, & \text{if } |P_t(x, y)| > L_{t-1}(x, y) \\ L_{max} \cdot \alpha_{RP} \cdot (1 + e^{i_t(x, y)})^{-1}, & \text{otherwise} \end{cases} \quad (3.4)$$

where α_{RP} is a coefficient to scale the decay function. While L_{max} is the upper boundary that $P_t(x, y)$ can reach. More specifically, if $P_t(x, y)$ manages to exceed $L_{t-1}(x, y)$, the consecutive local threshold $L_t(x, y)$ rises to L_{max} ; otherwise $L_t(x, y)$ decays exponentially and is updated with i , which is determined by the following equation:

$$i_t = \begin{cases} 1, & \text{if } P_t(x, y) > L_{t-1}(x, y) \text{ or} \\ & i_{t-1} \geq T_{decay} \\ i_{t-1} + 1, & \text{otherwise} \end{cases} \quad (3.5)$$

where the T_{decay} is a determining constant for how many frames that a local threshold decays according to equation (1) case otherwise. Subsequently, while values of activated photoreceptor cells are inherited by cells in the E layer at corresponding point, these values, with one image frame delay, flows into I layer as well, where inhibition is passed, elucidated

by

$$I_t(x, y) = \sum_i \sum_j P_{t-1}(x+i, y+j) \cdot w_I(i, j) \quad (3.6)$$

$$w_I = \begin{bmatrix} 0.125 & 0.25 & 0.125 \\ 0.25 & 0 & 0.25 \\ 0.125 & 0.25 & 0.125 \end{bmatrix} \quad (3.7)$$

where $I_t(x, y)$ represents the inhibition of the cell positioned at (x, y) at t moment. $w_I(i, j)$ indicates a 3×3 local convolutional kernel representing local inhibition weight, which allows local inhibition to pass through to its neighbouring cells, thus i and j shall not concurrently equal to zero. The following layer is S layer, where excitation transmitted from E layer and inhibition from I layer is summed by the following equation:

$$S_t(x, y) = E_t(x, y) - I_t(x, y) \cdot W_I \quad (3.8)$$

where W_I is a weight parameter constant. Here, outcomes of S cells, instead of being gathered immediately by the *LGMD* neuron, are injected into a group layer (G layer) to further enhance the developing edges derived from complex stimuli via a specialized convolutional operation, which is given by

$$[Ce]_t = [S]_t \otimes [w_e] \quad (3.9)$$

$$w_e = \frac{1}{9} \times \begin{bmatrix} 1 & 1 & 1 \\ 1 & 1 & 1 \\ 1 & 1 & 1 \end{bmatrix} \quad (3.10)$$

where \otimes is defined as a convolution operator, and w_e accordingly is the convolutional mask. The output Ce_t is then forwarded to G layer. Please note that Ce_t shall be partially discarded to match the magnitude of S_t . Capable of providing stronger input to the consecutive *LGMD* cell, G layer is explicit as follows:

firstly, raw data is calculated by

$$g_t = w^{-1}([S]_t * [Ce]_t) \quad (3.11)$$

where w^{-1} is a scalar for the Hadamard product of $[S]_t$ and $[Ce]_t$. The scalar is updated every frame by the following equation:

$$w = \Delta c + \max(\text{abs}[Ce]_t) \cdot C_w^{-1} \quad (3.12)$$

within which Δc is a small positive real number while C_w^{-1} is a constant, and $\max(\text{abs}[Ce]_t)$ extracts the maximum value within the matrix Ce_t .

Secondly, the raw g_t is further selected by

$$G_t(x, y) = \begin{cases} g_t(x, y), & g_t(x, y) \cdot C_{fa} \geq T_{fa} \\ 0, & \text{otherwise} \end{cases} \quad (3.13)$$

where C_{fa} denotes the fading coefficient that belongs to $(0, 1)$, and T_{fa} is the fading threshold. After the G layer, not only the edge information collected from approaching motion is further strengthened, but also the excitation collected from cluttered background is cancelled to a certain degree. The product G_t subsequently is conveyed to the *LGMD* neuron to be calculated by following equations divided into two steps:

$$K_t = \sum_x \sum_y \text{abs}(G_t(x, y)) \quad (3.14)$$

where firstly the summation of membrane potential, K_t , is calculated by sum every absolute value of pixel in G layer. Secondly the aforementioned summation is normalized utilizing a

sigmoid function stated below:

$$LGMD_t = (1 + e^{-K_t \cdot n_{cell}^{-1}})^{-1} \quad (3.15)$$

where n_{cell} counts photoreceptors on the retina. Once the output membrane potential of $LGMD$ neuron, which is normalised and limited in the range $[0.5, 1]$, exceeds the stationary threshold T_{lgmd} , one spike is fired:

$$spike = \begin{cases} 1, & \text{if } LGMD_t > T_{lgmd} \\ 0, & \text{otherwise} \end{cases} \quad (3.16)$$

Under physical circumstances, turning provokes enormous luminance change that triggers the LGMD model in a predominant manner. Hence, the Feed Forward Inhibition (FFI) mechanism is introduced together with lateral inhibition to suppress rapid luminance change caused by turning. It functions as the following equations:

$$F_t = n_{cell}^{-1} \cdot \sum_x \sum_y |P_{t-1}(x, y)| + \sum_i^{n_a} (\alpha_{t-1}^F \cdot F_{t-i}) \quad (3.17)$$

where α_{t-1}^F denotes a coefficient which belongs to $(0, 1)$, weighing the impact of previous F_{t-i} . Then the result F_t is compared with a threshold, T_{ffi} , which is updated to time by

$$T_{ffi_t} = T_O + \alpha_{ffi} \cdot T_{ffi_{t-1}} \quad (3.18)$$

where T_O is the original value of T_{ffi} and α_{ffi} is a scalar.

Compared with those methods that require more computational power such as objective detection and large-scale driving scene reconstruction[23], this LGMD1-based is acceptable in terms of accuracy and robustness while considerably low in algorithm complexity,

which retains the potential for being further embedded into low-energy consuming hardware platforms.

3.3 LGMD2 neural network with RP

As an interneuron of LGMD1, LGMD2 has its distinct characterization while retain some of the features of LGMD1 including responding strongly to approaching objects.

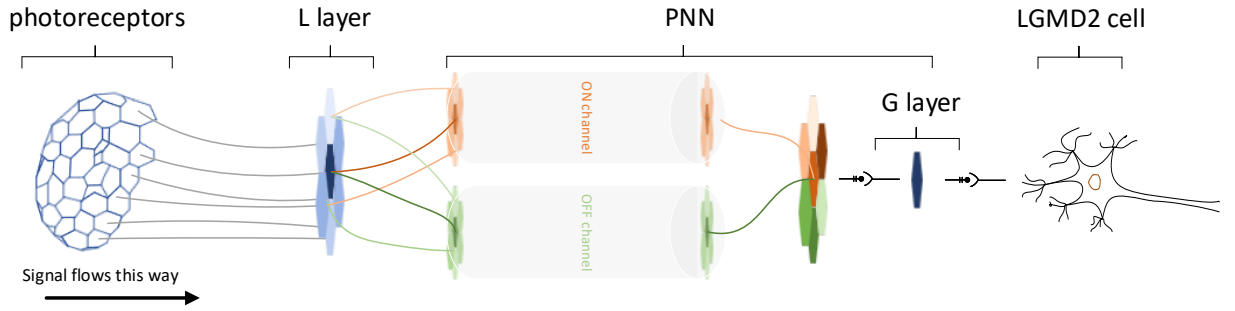


Fig. 3.3 Schematic diagram of our proposed LGMD2 method. The signals from photoreceptors firstly are injected to the L layer, where neural refractoriness happens, and secondly are separated into parallel ON & OFF channel (compared to the structure in Fig. 2.15). After that, edge-expansion information is enhanced by S and G layer. Finally, strong enough stimuli will activate LGMD2 neuron.

Thus, the first P layer is calculated by the change of luminance between two frames plus a temporal residual as follows:

$$P_t(x, y) = B_t(x, y) - B_{t-1}(x, y) + \sum_{n=1}^{n_p} \alpha_n \cdot P_{t-n}(x, y) \quad (3.19)$$

where $P_t(x, y)$ denotes the change of luminance at point (x, y) at the very moment t . The persistence of P_t lasts for n_p frames, and its strength decay over time, which is defined by α_n :

$$\alpha_n = (1 + e^n)^{-1} \quad (3.20)$$

The output of each P cell then is injected into the L layer, where the refractoriness steps in to limit the spike frequency. It can be described as below:

$$L_t^{on/off}(x,y) = \begin{cases} L_{max}, & \text{if } |P_t^{on/off}(x,y)| > L_{t-1}^{on/off}(x,y) \\ L_{max} \cdot \alpha_{RP} \cdot (1 + e^{i_t^{on/off}(x,y)})^{-1}, & \text{otherwise} \end{cases} \quad (3.21)$$

$$i_t^{on/off} = \begin{cases} 1, & \text{if } P_t^{on/off}(x,y) > L_{t-1}^{on/off}(x,y) \text{ or} \\ & i_{t-1}^{on/off} \geq T_{decay}^{on/off} \\ i_{t-1}^{on/off} + 1, & \text{otherwise} \end{cases} \quad (3.22)$$

where, same as in LGMD1 neural network, α_{RP} is a constant coefficient. After that, the output is passed on into two separated visual cue pathways, namely ON & OFF pathway.

$$P_t^{on} = P_t(x,y) + \alpha_r \cdot P_{t-1}^{on}(x,y) \quad (P_t(x,y) \geq 0) \quad (3.23)$$

$$P_t^{off} = -P_t(x,y) + \alpha_r \cdot P_{t-1}^{off}(x,y) \quad (P_t(x,y) < 0) \quad (3.24)$$

More specifically, the ON pathway accepts luminance increment with residual from its last moment of a small proportion (weighed by α_r), whilst the OFF pathway allows brightness decrement to flow into with a residual. This mechanism is also proved to be effective to encode motion detectors of other insect' brains including small target movement detectors of flying insects[42, 41].

In **respective** channel, the output of L layer, namely the 'refractorized' P , flows to its connecting E layer without temporal delay whilst goes to I layer with latency, which is determined by a time delay unit (see Fig 2.15). I cells subsequently are formed by convolving surrounding delayed excitations. The process is described as below:

$$E_t^{on/off}(x,y) = L_t^{on/off}(x,y) \quad (3.25)$$

$$\hat{E}_t^{on/off}(x,y) = \alpha_{on/off} E_t^{on/off}(x,y) + (1 - \alpha_{on/off}) E_{t-1}^{on/off}(x,y) \quad (3.26)$$

$$\alpha_{on/off} = \frac{\tau_{in}}{\tau_{on/off} + \tau_{in}} \quad (3.27)$$

$$I_t^{on/off} = \sum_{i=-1}^1 \sum_{j=1}^1 \hat{E}_t^{on/off}(x,y) W_{on/off}(i+1, j+1) \quad (3.28)$$

$$W_{on} = \begin{bmatrix} 0.25 & 0.5 & 0.25 \\ 0.5 & 2 & 0.5 \\ 0.25 & 0.5 & 0.25 \end{bmatrix} \quad W_{off} = \begin{bmatrix} 0.125 & 0.25 & 0.125 \\ 0.25 & 1 & 0.25 \\ 0.125 & 0.25 & 0.125 \end{bmatrix} \quad (3.29)$$

where $\tau_{on/off}$ stands for the delay time unit and τ_{in} for the time interval between consecutive frames of digital signals. $W_{on/off}$ is the ON channel convolutional mask. As shown in the Fig 2.15(b) and 3.27, within I layer, the spread latency of $E_t^{on/off}(x,y)$ to its corresponding position is the shortest, thus the weight is highest, while on the contrary to its diagonal is the longest accordingly making the weight the lowest.

The excitation and inhibition in each channel is firstly linearly summarized, and subsequently conveyed to the S layer:

$$S_t^{on/off}(x,y) = [E_t^{on/off}(x,y) - w^{on/off} \cdot I_t^{on/off}(x,y)]^+ \quad (3.30)$$

$$S_t(x,y) = \theta_{on} \cdot S_t^{on}(x,y) + \theta_{off} \cdot S_t^{off}(x,y) + \theta_0 \cdot S_t^{on}(x,y) \cdot S_t^{off}(x,y) \quad (3.31)$$

where the operation $[x]^+$ compares x with 0 and winner takes all, $\theta_{on/off}$ is defined to be S cells' preference, and θ_0 allows to mediate the impacts that contrast of each channel imposes. $w^{on/off}$ is time-varying local biases to control the intensity of inhibitory flows, which is related to the PM mechanism. Due to rapid luminance change resulted from turning, the photoreceptor can be strongly activated and false positive spikes could be fired in its wake. However, unlike LGMD1, from the perspective of neuroscientific anatomy, there

is not adjacent pathway in LGMD2 like FFI to suppress this 'false alert'. Instead, the PM mechanism is introduced to achieve this:

$$PM_t = n_{cell}^{-1} \cdot \sum_x \sum_y |P_{t-1}(x, y)| \quad (3.32)$$

$$\hat{PM}_t = \alpha_{PM} \cdot PM_t + (1 - \alpha_{PM}) \cdot PM_{t-1} \quad (3.33)$$

$$\alpha_{PM} = \frac{\tau_{in}}{\tau_{PM} + \tau_{in}} \quad (3.34)$$

where n_{cell} denotes the total of P cells, α_{PM} is the weighing factor, τ_{PM} stands for a delay time constant in millisecond. Then the $w^{on/off}$ is derived from:

$$w_{on} = \max(w_1, \frac{\hat{PM}_t}{T_{PM}}) \quad (3.35)$$

$$w_{off} = \max(w_2, \frac{\hat{PM}_t}{T_{PM}}) \quad (3.36)$$

where w_1, w_2 are the predefined baselines of bias in ON and OFF channel respectively and T_{PM} is a threshold constant. Same as in LGMD1 and Eq 3.9-3.13, edge information derived from the first several layer is further enhanced by G layer and obtain the consequence $G_t(x, y)$. The LGMD2 cell firstly collects the consequence:

$$k_t = \sum_x \sum_y G_t(x, y) \quad (3.37)$$

and secondly normalises it to $[0.5, 1)$ as follows:

$$K_t = (1 + e^{-k_t \cdot (n_{cell} \cdot \alpha_{LGMD})^{-1}})^{-1} \quad (3.38)$$

Where α_{LGMD} is a scale coefficient. To further shape and sharpen the LGMD2's selectivity and output pattern, an SFA mechanism is implemented as below equation:

$$LGMD_t = \begin{cases} \alpha_{SFA} \cdot (LGMD_{t-1} + K_t - K_{t-1}), & \text{if } (K_t - K_{t-1}) \leq T_{SFA} \\ \alpha_{SFA} \cdot K_t, & \text{otherwise} \end{cases} \quad (3.39)$$

where T_{SFA} denotes the threshold for SFA mechanism, which is a small real number, and α_{SFA} is a coefficient, defined as the adaption rate to visual movements, is collected as:

$$\alpha_{SFA} = \frac{\tau_{SFA}}{\tau_{SFA} + \tau_{in}} \quad (3.40)$$

where τ_{SFA} is a delay time constant in millisecond.

3.3.1 Parameter settings

Note that the L_{max} depends on the gray-scale of the monochromatic images converted from RGB images. In MATLAB, the maximum is 255 so accordingly the L_{max} is set to the same. The α_{RP} is set to 2 to make the ARP stage is included in entire process of neural refractoriness. The T_{decay} is set to 7 since the naturally decaying dynamic threshold is less than 0.5, meaning the impact of the dynamic is as low as less than 0.002. Thus, it is deemed to have returned to resting potential and the local threshold will manually set to 0 to save computing resources. n_{cell} represents how many photoreceptors in the whole visual field, depending on the resolution of input video signals. The other parameters in LGMD1 are inherited from [45], whilst the remaining in LGMD2 are from [11]

Table 3.1 The Parameter Settings for LGMD1 and LGMD2 neural network

parameters	description	in LGMD1	in LGMD2
L_{max}	Maximum of the Link layer threshold	255	255
α_{RP}	Coefficient to scale the decay function	2	2
T_{decay}	Threshold life length	7	7
W_I	local inhibition weight kernel	0.3	0.3
Δ_C	A small real number	0.01	0.01
C_w	A small positive real number	4	4
C_{fa}	Coefficient in G layer	0.5	0.5
T_{fa}	Threshold in G layer	15	15
T_O	Initial value of FFI threshold	7.5	7.5
α_{ffi}	FFI threshold growing coefficient	0.02	0.02
T_{lgmd}	Membrane potential threshold	0.7	0.7
i_0	Index indicating decay time in L layer	1	1
α_r	A residual weight factor	N/A	0.1
$\theta_{on/off}$	A weight factor for ON/OFF in S layer	N/A	1 / 0.5
θ_0	A contrast mediation factor	N/A	1
n_p	Residual length in LGMD2 P layer	N/A	2
$\tau_{on/off}$	Time delay unit (ms)	N/A	See Fig2.15(b)
τ_{SFA}	A delay time constant in (ms)	N/A	500
τ_i	Interval between consecutive frames (ms)	N/A	depending on signal sampling rate
w_1	Baseline of bias in ON channel	N/A	1
w_2	Baseline of bias in OFF channel	N/A	0.5
T_{PM}	A threshold constant	N/A	10
n_{cell}	Number of photoreceptors	unknown	unknown

Chapter 4

Experiments

In this chapter, firstly the dataset used for offline tests is introduced. Secondly, aiming at precisely recognising the moment when collision happens, the systematic experiments for each proposed LGMD neural network are divided into three parts, namely 1) the feasibility test, in which the proposed LGMD neuron endowed with refractoriness is tested with certain computer-generated stimuli and one real-world stimulus where a black ball rolling, colliding onto the camera lens. The results are then compared with those collected from previous corresponding LGMD model to see whether the proposed LGMD neural network work properly with neural refractoriness; 2) tests against ultra-fast approaching objects, utilizing several clips where the same black ball flying, colliding onto the camera lens. The statistic results are plotted as a confidence plot, compared with results from previous LGMD model to see whether positive impacts are made; 3) tests against Gaussian noise and Salt & Pepper noise respectively at various density. Statistic data are visualized to see if the proposed neural refractoriness to some extent improves previous model's resisting against noisy signals. Evaluation of numerical mimicking neural refractoriness can be accomplished.

4.1 Dataset

Previously, while exploring performance of LGMD neural networks, researchers utilize video signals, where the velocity of objects is usually as low as no more than 1 m/s , as their offline experimental materials. As for the real-time tests carried on a micro-robot, the velocity is usually measured in centimetres. Thus, in this study to explore how refractoriness affects the performance of LGMD model when faced with ultra-fast objects on a colliding course, videos recorded under experimental circumstances, where the velocity of the incomings is more than 5 m/s , up to around 9.6 m/s , are utilized. As the RP is fairly short period of time [4], aiming at mimicking the actual transitory duration of RP, a high-speed dynamic camera, GoPro8, is used to sample the processes of a black ping pong ball approaching and hitting its lens at sampling rate of 240 Hz , that is to say, capture one frame every 4.1667 millisecond, 8 times as quick compared to 30 Hz which is the sampling rate previous works adapts. In this way, the actual duration of RP is approached closer to.

In subsection 4.2.1, 20 video clips shot on GoPro8 are included. Individual clip at sampling rate (or frame rate) 240 Hz is resized to resolution of 320×180 from 1920×1080 , then decimated to sampling rate of 30 Hz and 24 Hz . To lower the sampling rate, designated frames from original videos are extracted according to the targeting frame rate. Taking 120 Hz frame rate for example, every $\frac{240\text{Hz}}{120\text{Hz}}$ frames makes up one 'frame set', within which every 1^{st} frame is used to form new clips. Then frames of the same amount that cover the whole approaching course are intercepted to be input as signals.

In subsection 4.2.1, the same 20 clips are then polluted by Gaussian noise or Salt-Pepper noise at different Signal-to-noise ratio (SNR). Some snapshots for visualising the noise signal are shown in Fig. 4.1 and 4.2.

A computer-generated simulative video is used as well, where a black square at the heart begins to grow at 15^{th} frame and pauses at 36^{th} frame within grey background.

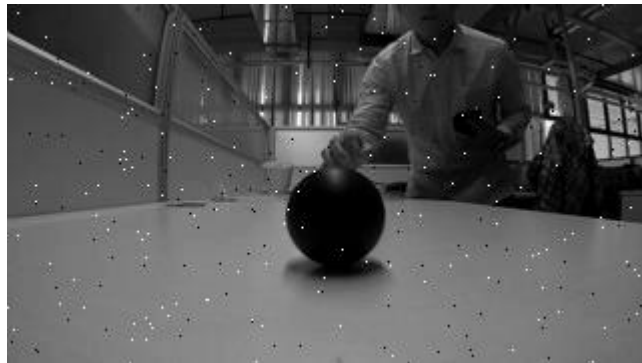
Fig. 4.1

Salt & Pepper noise

Density = 0.001



Density = 0.005



Density = 0.01

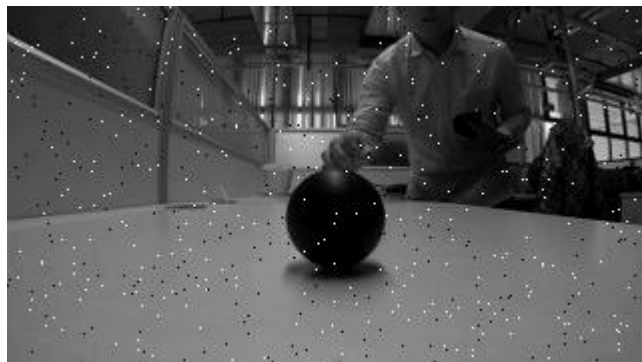


Fig. 4.2

Density = 0.05



Gaussian noise

Average = 0.001, variance = 0.01



Average = 0.01, variance = 0.01



4.2 Experiment evaluation

In this section, the target for our proposed methods is to more accurately tell the moment that collision happens, and to avoid too premature spikes when the object is still far away, not huge enough and threatening enough to fire spikes, as well as to avoid too postponed spikes when collision has already happened.

In the subsections of 'Effectiveness against Ultra-Fast Objects', the 'ultra-fast' is referring velocity higher than 3.6 m/s [43], the usual speed of a desert locust, up to around 3 times the speed.

4.2.1 RP in LGMD1 experimental evaluation

In this section, the experimental results are illustrated step-by-step, divided into 3 steps: a) feasibility of the proposed model with RP mechanism, b) effectiveness of proposed model against ultra-fast inbound objects and c) performance against noise-polluted signals.

Feasibility of RP

Firstly, the model is tested with aforementioned computer-generated simulative signal and GoPro-captured video to validate the feasibility of integrating RP mechanism with classic LGMD model. Results are illustrated by Fig.4.3 and Fig.4.4 clearly. The orange curves represent the normalized responses of LGMD neuron (Eq. 3.15) handled by L layer and RP mechanism in our proposed model, while the blue ones show output of classic LGMD model. The green horizontal lines are T_{lgmd} which is set to recognize collision. For computer-generated clips, neural refractoriness holds the LGMD1 neuron for 3 frames, whilst for the real-world stimulus, true collision timing is postponed for 8 frames until the object is large enough to be recognised in the colliding course. From the outcomes, it can be noticed that RP mechanism causes LGMD observes and spikes for collision with acceptable several frames delay, which accurately narrows down the range of collision, and so, firing a premature spike

when the approaching object is still distant and not large enough can be efficiently avoided. It is also worth noticing in Fig.4.4 that RP silences the LGMD1 neuron while the object is far away from the camera, hence it can be safely deduced that neural refractoriness makes progress in telling the actual timing of collision.

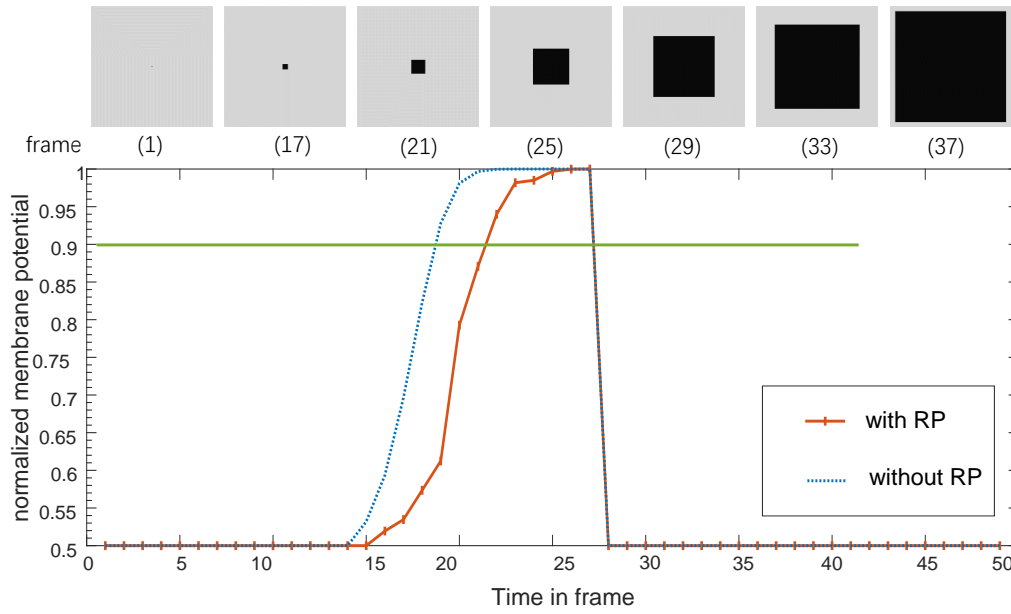


Fig. 4.3 Examples of snapshots of the computer-generated video with corresponding frame number tagged below. With the black square grows, the responses gets more intensive and trespasses the T_{lgmd} (set to 0.9 for simulative signals) until reaches the upper boundary. Orange curve and blue dashed curve clearly show that both models succeed in extracting the motion pattern of approaching.

Effectiveness against Ultra-Fast Objects

Here when 'ultra-fast' is talked about, higher velocity up to 10 m/s is referred to, which triggers the LGMD neuron falsely and repeatedly. By lowering sampling rate of the 20 GoPro8-shooting videos, continuous motion is further discretized in time dimension, thus objects seem to move faster if the lowered sampling rate mapped again from low to higher, due to comparatively more immense difference between two frames.

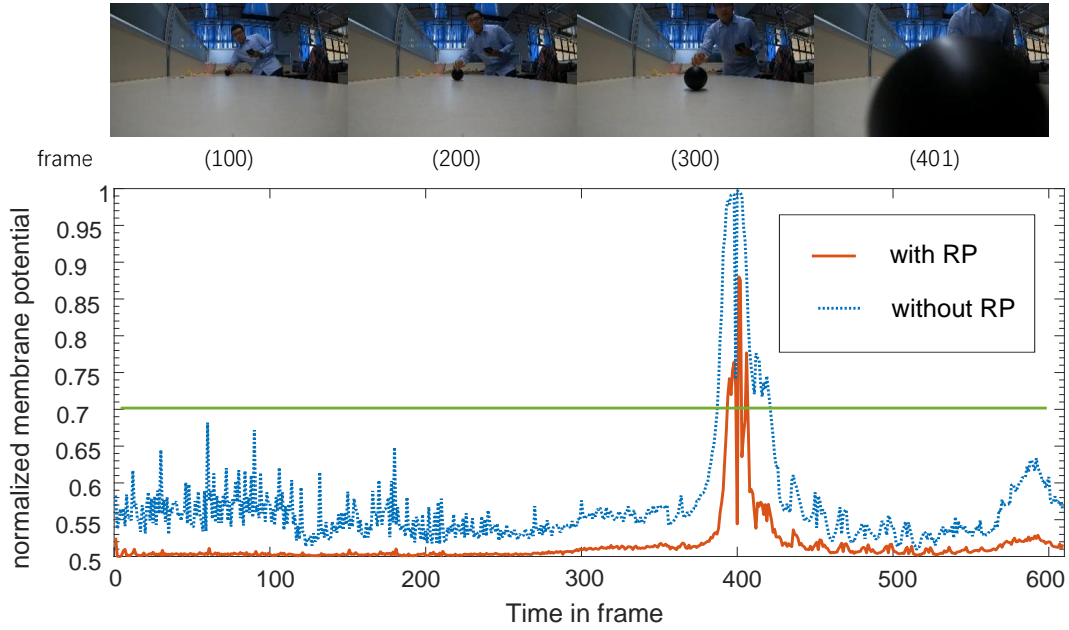


Fig. 4.4 Snapshots of the recorded signal at 240 Hz with frame number tagged below. At an average velocity of 0.8727 m/s and initial velocity of 0 m/s , the black ball starts to roll to camera lens from 1 m away at 122^{nd} frame, and hits it at 401^{st} frame, followed by frames where the ball goes backwards. 0.7 is set as T_{lgmd} in Eq.3.16 for real-world signals.

From the results of comparative experiments calculated by Eq.3.15, it can be noticed that when signals are sampled at 240 Hz , both models succeed in recognizing impending collision during the collision zone (between by 2 red dashed lines), but without RP, LGMD neuron produces spikes several frames earlier.

For low sampling rate signals, both models are tested with 30 Hz as well as 24 Hz . Though classic LGMD without RP mechanism is activated during collision zone, it fires spikes when the objects are still far away from the camera lens, meaning false alert, while our proposed model with RP notifies the right collision.

It is also worth paying attention to the standard deviation in the confidence plot outside the collision zone, where LGMD is not supposed to fire, our model demonstrates effectiveness on reducing the standard deviation of membrane potential and silencing the neuron in Fig.4.5, and in Fig.4.6a and Fig.4.6b and in the wake of this, our proposed refractoriness leads to

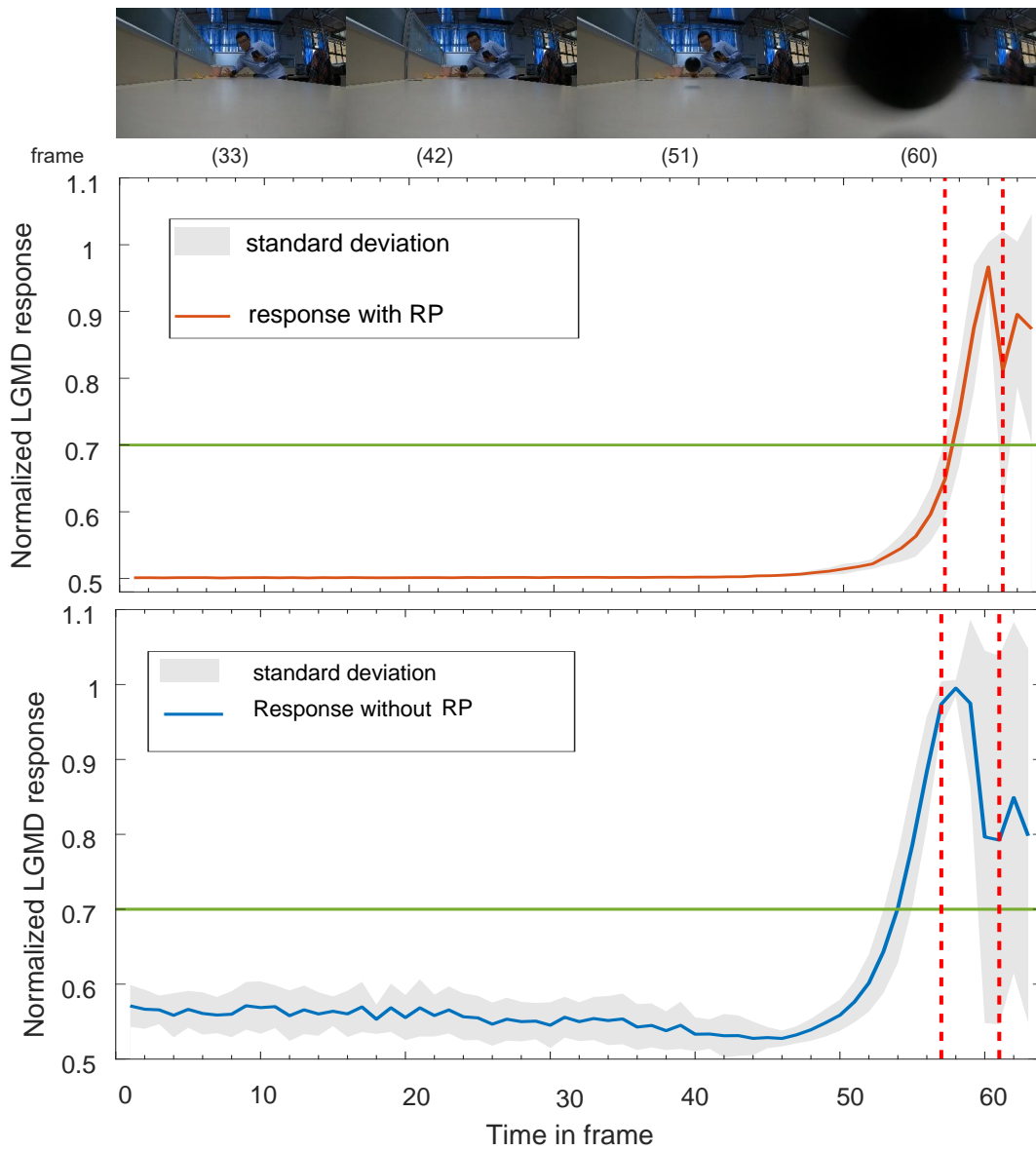


Fig. 4.5 Example snapshots of one of video signals and statistical results below frame number tags. T_{lgmd} illustrated by horizontal green line. Between two red dashed lines are collision zone. The orange curve and blue curve represent the average LGMD membrane potential at every corresponding frame or moment in 20 video clips respectively. Light grey area covers the standard deviation of all signals at a certain frame. Collision is reported by both models. Orange curve shows collision is extracted while blue one reports collision several frames earlier. The orange curve also shows stationary property before collision, compared with the blue one.

more stable collision perception. RP also shows influence on weakening the fluctuation but not that obvious compared with high sampling rate signals. This, to some extent, suggests that useless and small edge expansion patterns may have been filtered while continuous expansion reserved for further collision perception.

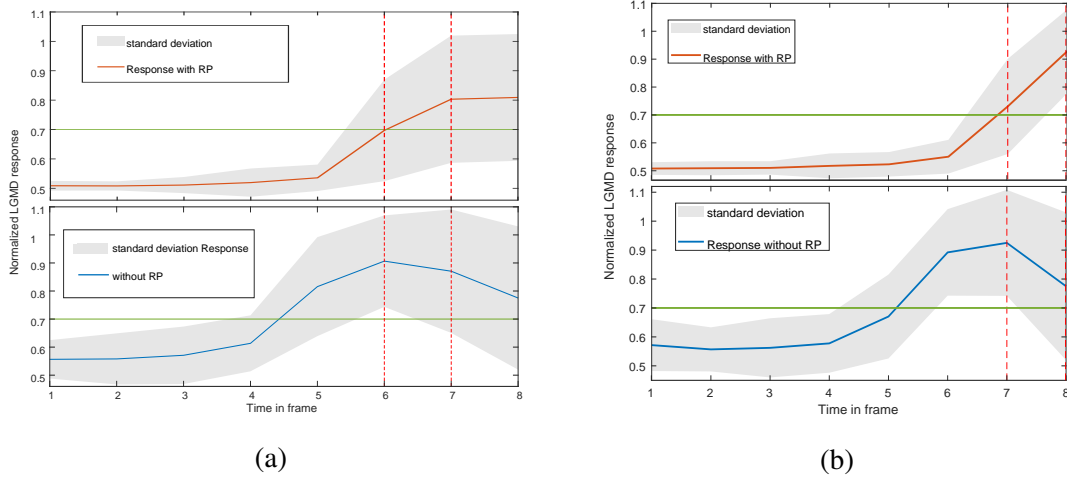


Fig. 4.6 Statistical results of signals at sampling rate 30 and 24 Hz . Whilst the previous LGMD1 neural network fails to generate correct spikes within the annotated collision zone, our proposed method retains it functionality of precisely firing spikes accurately within the collision zone, with less premature or postponed spikes.

Performance against Noisy-Polluted Signals

Subsequently, PR is tested for noise resistance ability, with the same 240 Hz signals used in subsection 4.2.1 polluted by either Gaussian noise or Salt-Pepper noise. Some of our experimental results show delightful efficacy on resisting the low-strength noise such as Gaussian noise (Fig.4.7). Although compared to classic model, RP mechanism helps to purify contaminated signals, it is still challenging to extract collision and approaching motion pattern when SNR drops as shown in Fig.4.8.

4.2.2 RP in LGMD2 experimental evaluation

Similarly, the LGMD2 network is tested with refractoriness enabled step by step. In this section, vertical axis represents the normalized LGMD2 membrane potential and horizontal axis is the time in frame.

Feasibility of RP

Due to LGMD2 owning its distinct features, for testing the feasibility of integrating RP with LGMD2 neural network, three sets of computer-generated stimuli plus one recorded in against real-world background are used. The first set is one dark square or one bright square

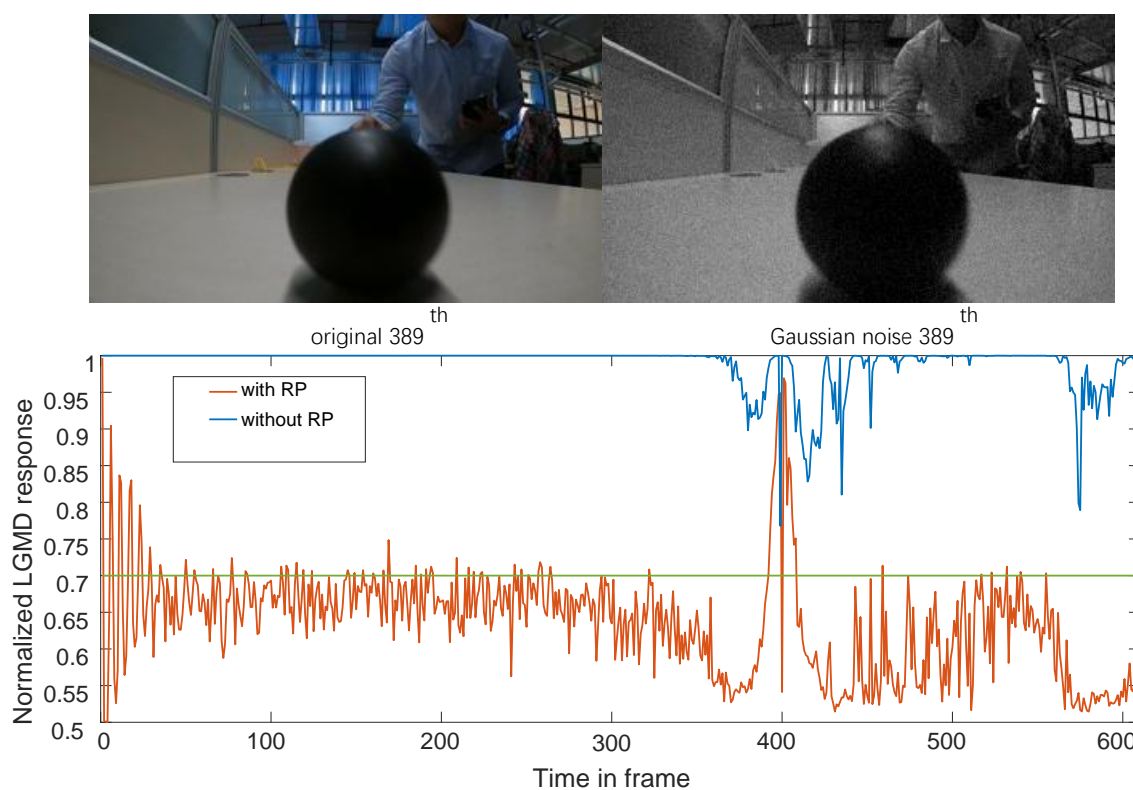


Fig. 4.7 Snapshots of 389th frame from original video and Gaussian-noise-contaminated video. The orange curve represents LGMD membrane potential (referring to Eq.3.15) with RP mechanism, comparatively blue one without RP. While most of the blue curve stays at 1, orange curve can be easily distinguished for the peak at 401st frame with violent fluctuation within first 40 frames.

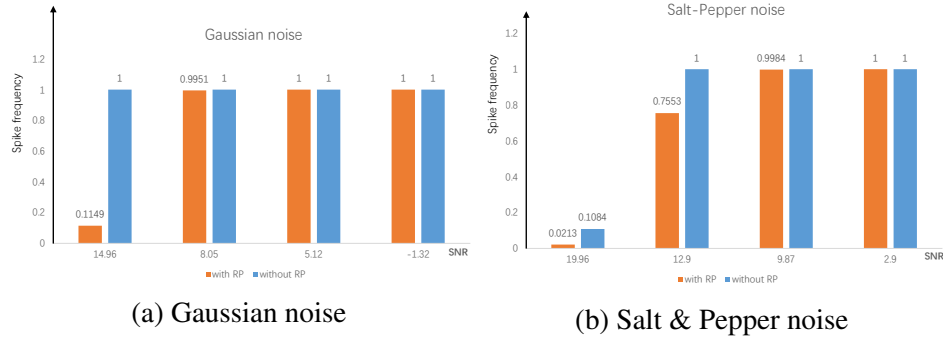


Fig. 4.8 Here, spike frequency is the product of amount of *spike* divided by amount of frames. (a) Orange bars illustrate that, spike frequency with RP mechanism interfering is low at SNR equalling 14.96, while blue ones show that LGMD is compromised by Gaussian noise. (b) Against low level Salt-Pepper noise, both models work properly and observe collision successfully. Comparatively, RP mechanism improves LGMD in terms of noise resistance.

zooms in and zooms out respectively against brighter background or darker background correspondingly (Fig. 4.9 top). The zooming in can be considered as objects approaching and zooming out is recession. The second set includes a dark rectangle or a bright rectangle is elongated or shortened respectively against brighter or darker background accordingly. These elongation and shortening process visually resembles translating motion pattern but the main body is larger than the field of view (see snapshots in Fig 4.10), compared to Fig 4.19. The last set contains a dark rectangle move at the same speed translating from left to right or reversely(4.19). The real-world clip refers to Fig 4.12.

From Fig4.9 to 4.11, it can be clearly seen that, with neuronal refractoriness limiting the neuron firing pattern, LGMD2 neural network works properly and succeeds in detecting the edge-expansion, namely the collision. Subsequently, the neural network is tested with the same the clips used in testing LGMD1 (see Fig4.4) recorded against real-world background (see Fig4.12). Compared with the output from the classic LGMD2 model, output of our proposed method shows much less fluctuation before collision is detected, and though shows lower membrane potential, the collision is successfully recognized.

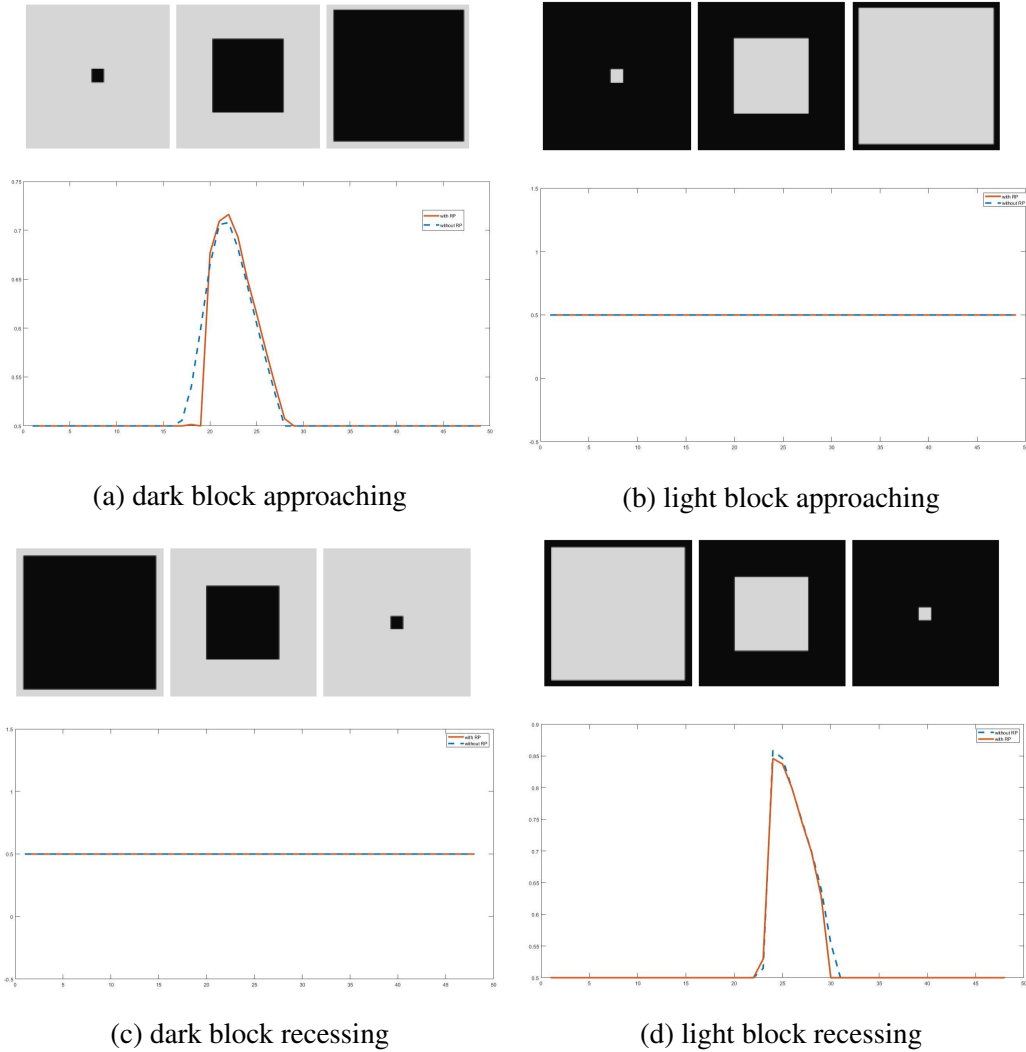


Fig. 4.9 Top of each sub-figure is some snapshots at certain frames. The experimental results are shown in the bottom, where the orange curve is LGMD2 neural network output with RP enabled, whilst the dashed blue curve is the output of classic LGMD2 model.

Effectiveness against Ultra-Fast Objects

With the same video clips used to test the performance of LGMD1 neural network when the incoming object is at ultra-fast velocity(see Fig 4.5, 4.6a, 4.6b), LGMD2 neural network is tested with the same stimuli. Statistical results are illustrated in Fig 4.13 to 4.15.

In Fig 4.13 and 4.14, collision is reported in time, which means the classic LGMD2 neural network, with or without refractoriness mechanism, is equipped with the ability to

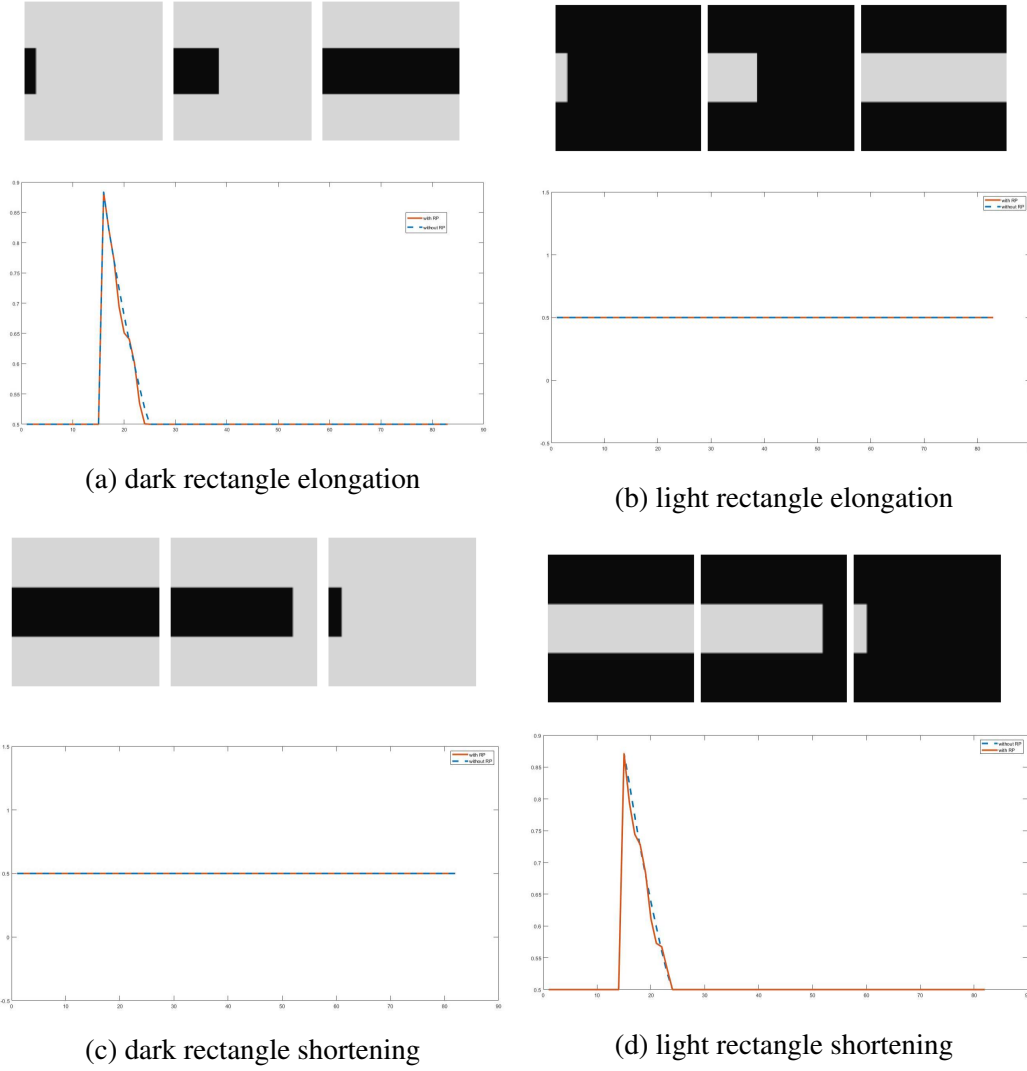
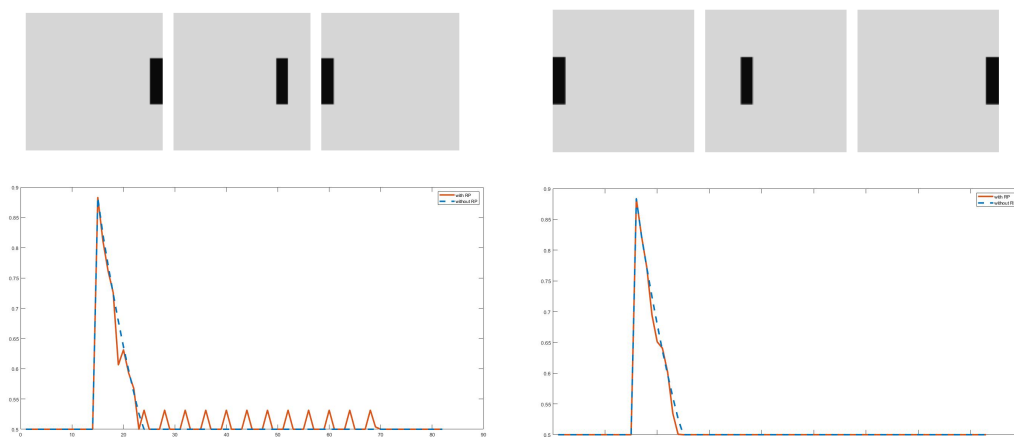


Fig. 4.10 Orange curves in each figure represents the outputs of our proposed method, whilst blue dashed lines represent those of classic LGMD2 membrane potential.

recognize impending collision that happens quickly. It can be deduced from the vertical axis that, with neuronal refractoriness, LGMD2 is less activated than the one without it. However, things are different when it comes to lower sampling rates. When the sampling rate is down to 60Hz , our proposed method, though trespass the threshold for true collision, half of the confidence area (as represented by light gray area) is under the threshold. Lowering the sampling further, both model fails to tell most of the collision pattern.



(a) dark rectangle translating to the left edge (b) dark rectangle translating to the right end

Fig. 4.11 As orange curve in (a) shows, our proposed model results in fluctuation after the motion pattern is extracted, when the neuron shall be silenced.

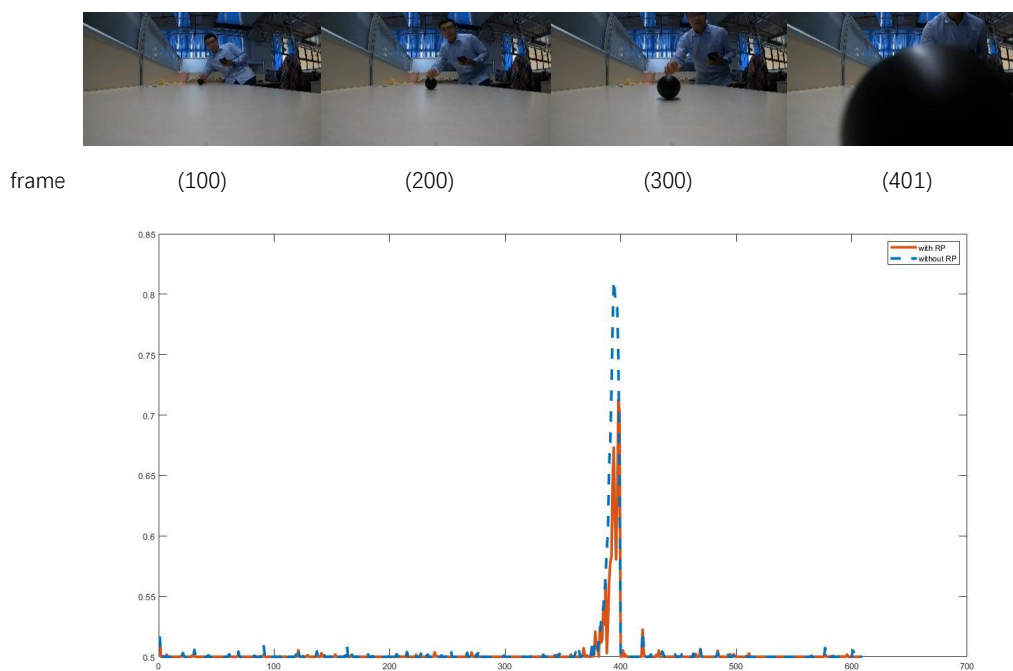


Fig. 4.12 The orange curve represents output of LGMD2 neural network with neuronal refractoriness enabled, while the blue dashed line is the output the classic LGMD2 model. The two curves imply that integration of LGMD2 model and neuronal refractoriness mechanism may be a potential way to further improve LGMD2 neural network's reliability and robustness for detecting low-speed objects on a colliding trajectory.

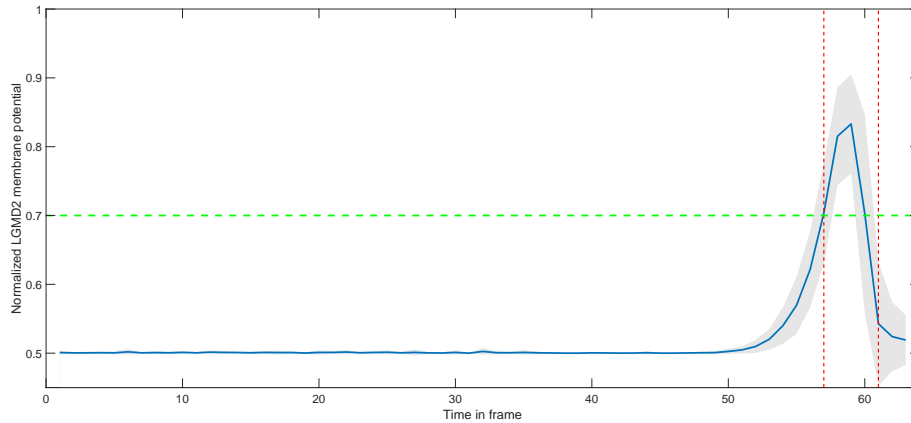


Fig. 4.13 Membrane potential of one previous work of LGMD2 neural network without neural refractoriness. Between the red dashed lines are when collision occurs. The green dashed line is the threshold chosen to tell true collision (below the same). The blue curve represent the average LGMD2 membrane potential at every corresponding frame or moment in 20 video clips respectively. Light grey area covers the standard deviation of all signals at a certain frame.

Performance against Noisy-Polluted Signals

For offline experiments on the LGMD2 with refractoriness, the same computer-generated video clips, where various motion pattern are displayed, are utilized together with one clip recorded by a Gopro8, where a blackened ping pong ball flies to the camera lens from 1 meter away at the speed around 1m/s.

Against the Salt & Pepper noise:

the key factor of Salt & Pepper noise is its density. Two density values are selected, i.e. 0.01 and 0.001 which means 1% and 0.1% pixels within every frame carries incorrect information, to obtain the normalized LGMD2 outcomes. It can be noticed from Fig 4.17 to 4.20, 4.20 in particular, that 1) with density increases (wrong information becomes more), the harder for LGMD2 to recognize collision; 2) high-density noise triggers the visual neuron at the beginning and then be suppressed. It is deduced that it's the photoreceptor mediation (PM) mechanism imposes its influence on this by adapting to the highly dynamic background; 3) with the same density, there is hardly difference of LGMD2 neuronal potential between

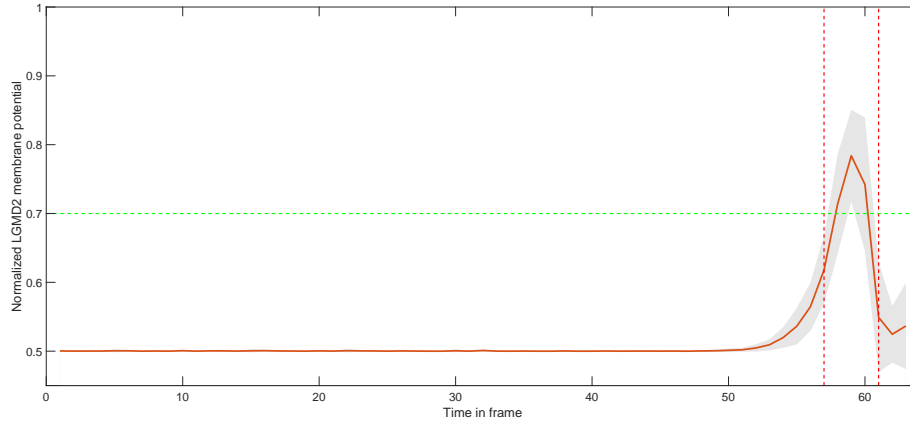
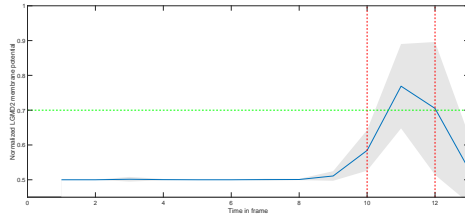
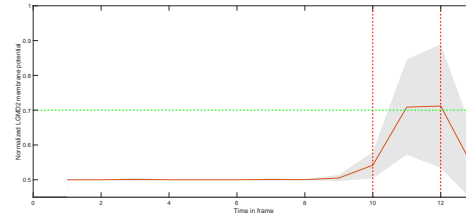


Fig. 4.14 Membrane potential of the proposed neural refractoriness integrated with previous LGMD2 neural network. Two red dashed lines indicates the temporal collision zone. The orange is the average LGMD2 membrane potential at certain frame. Light grey area covers the standard deviation of all signals.



(a) At sampling rate 60HZ

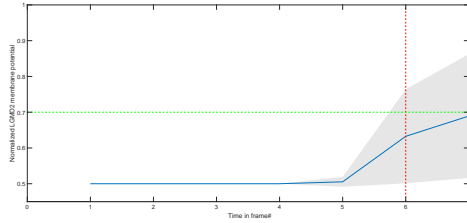


(b) At sampling rate 60HZ

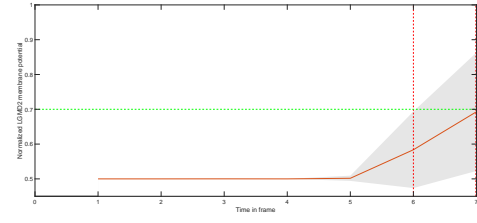
Fig. 4.15 Normalized membrane potential curve of classic LGMD2 neural network, without neural refractoriness. The sampling rate of the input is lowered to 60Hz, so that the incoming collision happens in seemingly much quicker than sampling rate of 240 Hz. Similar as results above, around half of the collision can be recognized.

with RP and without RP; 4) If the initial spikes are neglected, the firing pattern is basically similar to the one when there's no contaminating noise. The 2), 3) and 4) might be supportive observation for the efficacy of PM mechanism.

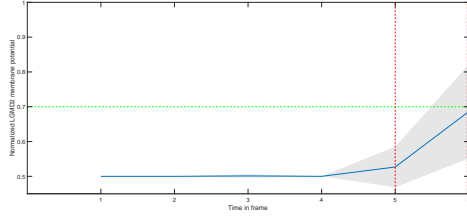
Against Gaussian noise: for test RP's impacts on LGMD2' resistance of noise signals, the same three sets plus one real-world clip are utilized. There are two factors regarding the SNR of Gaussian noise, namely the 'average' and the 'vriance'. From previous efforts made to test LGMD1 against Gaussian noise, it is learnt that the average barely influence the



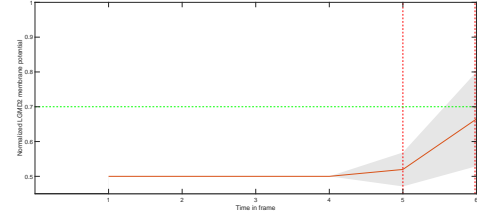
(a) At sampling rate 30HZ



(b) At sampling rate 30HZ

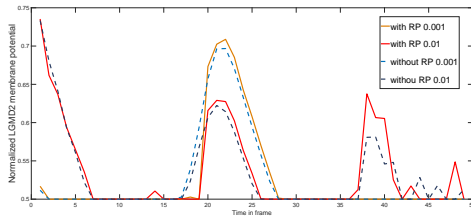


(c) At sampling rate 24HZ

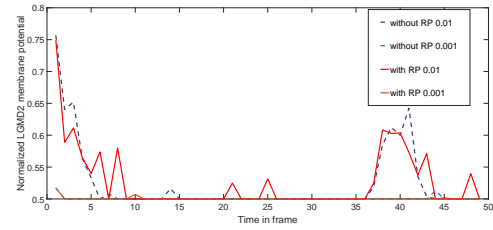


(d) At sampling rate 24HZ

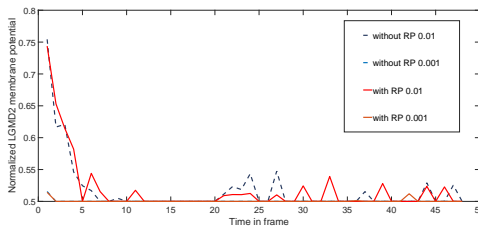
Fig. 4.16 (a) and (b) indicate the normalized LGMD2 membrane potential curve with input videos at sampling rate of 30Hz, while (c) and (d) show that with input sampling rate at 24Hz. Both sets of experiment show that most collision can not be extracted, even with neuronal refractoriness enabled.



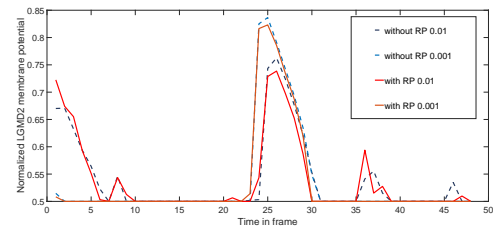
(a) dark approaching



(b) light approaching



(c) dark recession



(d) light recession

Fig. 4.17 The normalized LGMD2 membrane potential curves are divided into two types. One is cool colour tone, showing model outputs without RP. The other is warm colour tone, showing outputs with refractoriness. 0.01 and 0.001 are referred to as different density values set for Salt & Pepper noise.

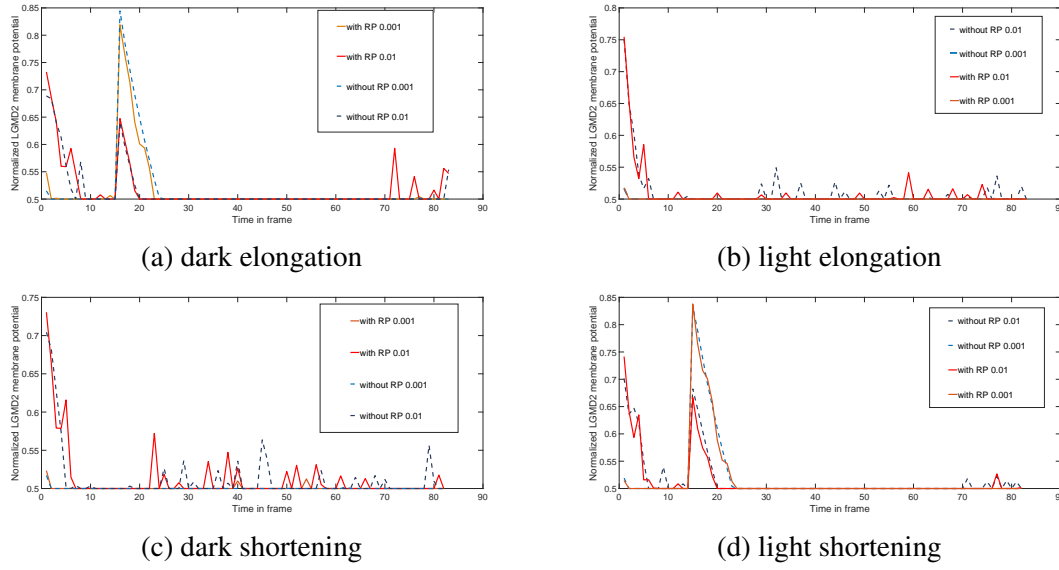


Fig. 4.18 The blue dashed curves show classic LGMD2 membrane potential, while red ones and orange ones show membrane potential of our proposed method. Though both models show similar firing patterns as those in the feasibility test, high density S & P noise stimulates LGMD2 cell to fire at first few frames.

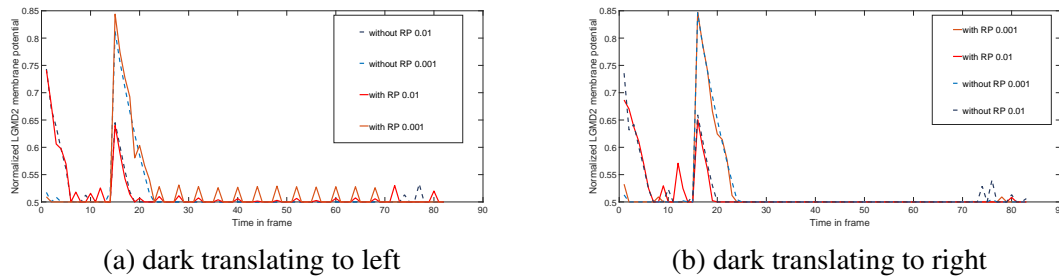


Fig. 4.19 With the same noise density, there is a little difference between with RP and without RP. In (a), the a few similar fluctuation from our proposed method under S & P noise of 0.001 density can be noticed.

outcomes. Thus, the ‘average’ is fixed to 0.01, and 0.001, as well as 0.01, is selected as the variance.

From the experimental results shown in Fig 4.21 to 4.24, the following can be concluded:

- 1) contaminated input signals make LGMD2 neuron spike at first, then silence itself rapidly;
- 2) though the LGMD2 neuron firing pattern against noise seems to be like the one without noise, the threshold for true collision is not trespassed, with or without neural refractoriness,

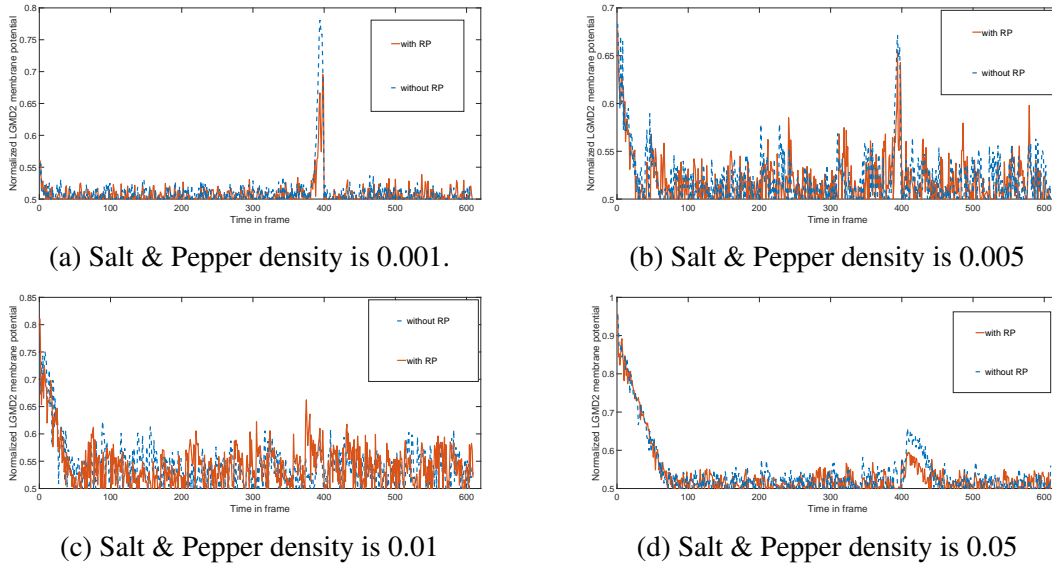


Fig. 4.20 Here the same signal in 4.7 is used to test LGMD2's resistance for various density Salt & Pepper noise. High density noise will trigger the LGMD2 cell at first and then be adapted. (a) Orange curve shows normalized membrane potential of our model, while blue dashed curve show the one of classic LGMD2 potential. Both models apparently discriminate the collision at right moment. (b) Fluctuation becomes more before and after collision is detected. (c) Both fail to tell collision. (d) Membrane potential increases sharply but still fails to reach the threshold for collision. With density increases, it becomes harder and harder to activate the LGMD2 cell to tell true collision.

which means the RP mechanism fails to benefit LGMD2 neuron even in a subtle manner.

Both neural networks cannot work properly against Gaussian noise.

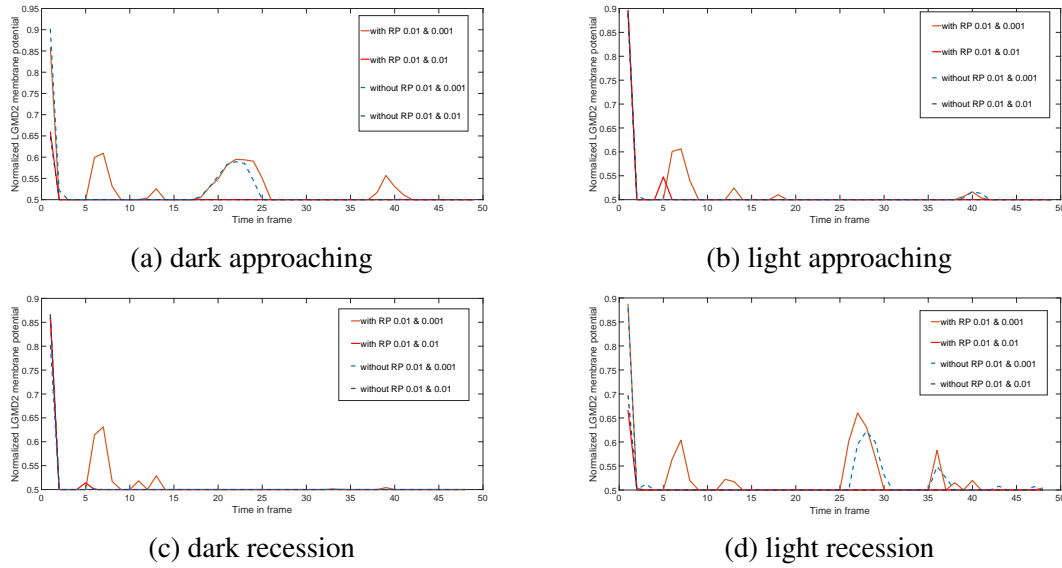


Fig. 4.21 Different from experimental results from above feasibility test, LGMD2 generates spikes at first, and then few irregular fluctuations. it can be notice from 4 sub-figures that, when the motion pattern or the background is the same, high level Gaussian noise stimulate LGMD2 neuron much less strong than low level one does.

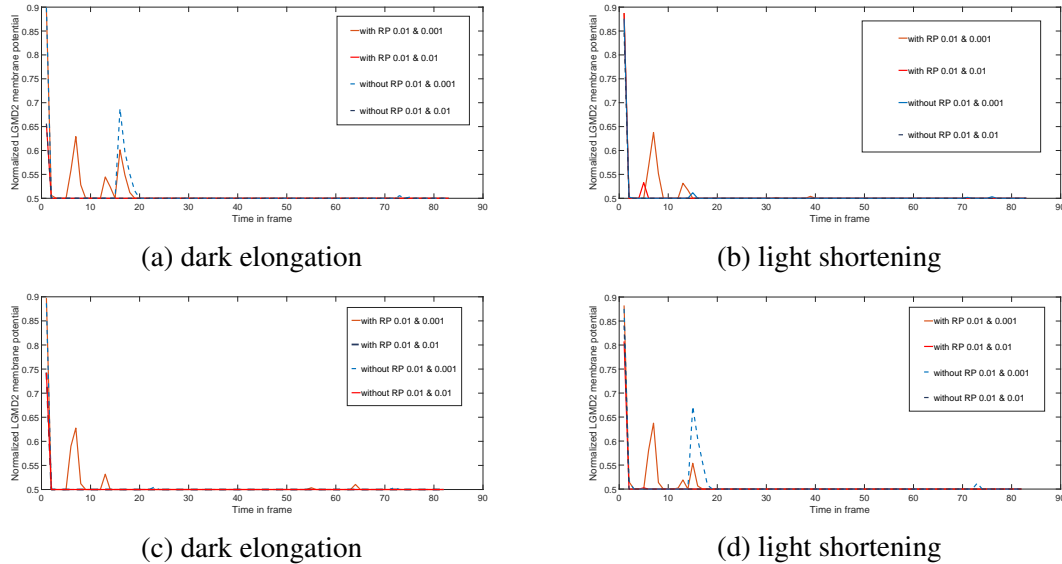
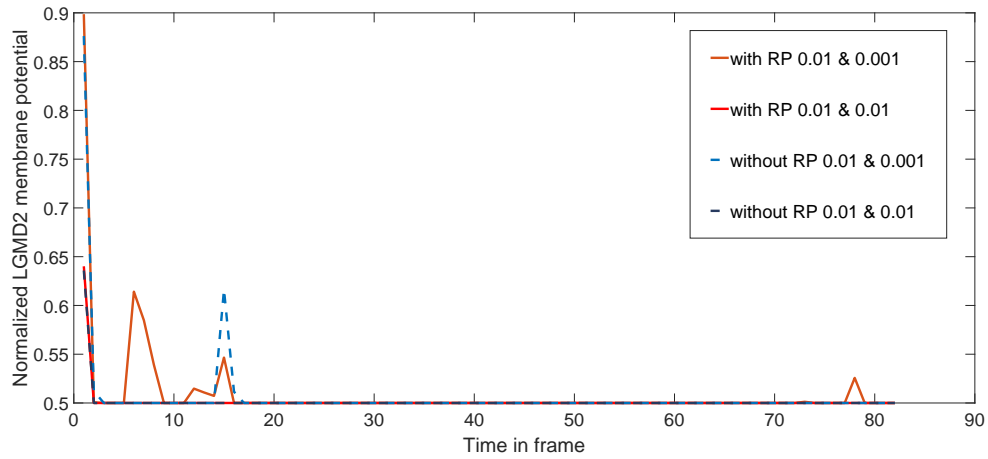
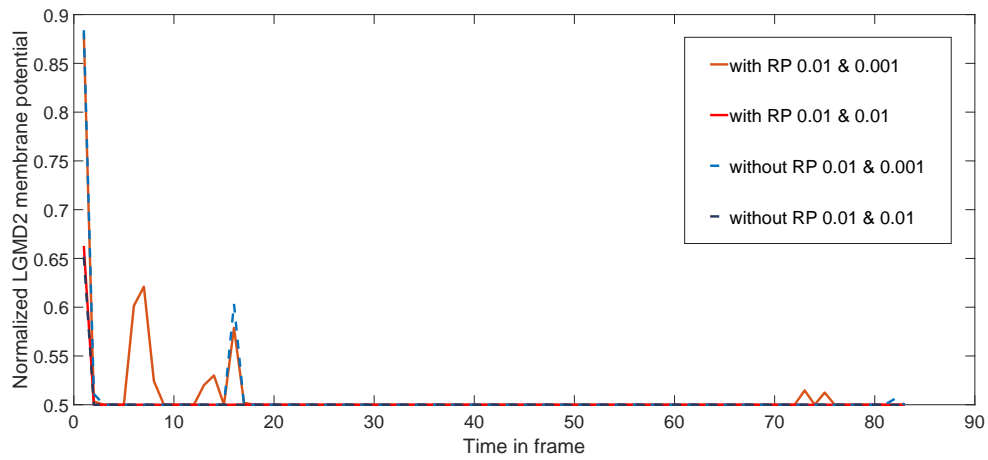


Fig. 4.22 The noise signal activates LGMD2 neuron strongly, and consequently with a few irregular fluctuation, the membrane potential comes to resting state.

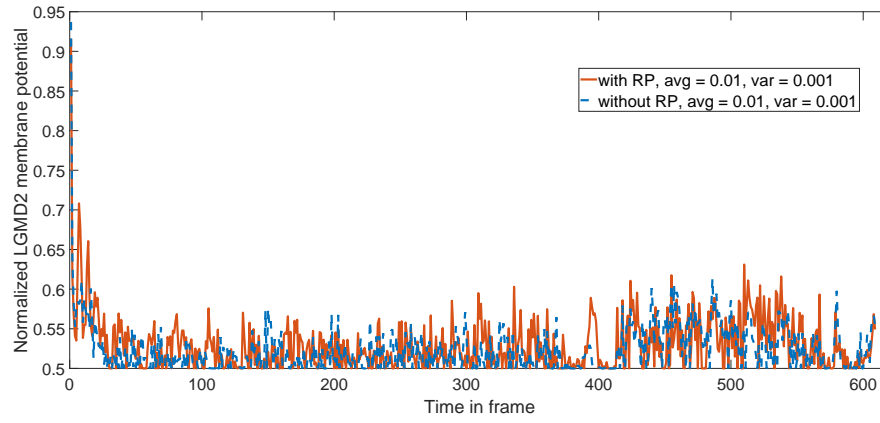


(a) dark translating to the left

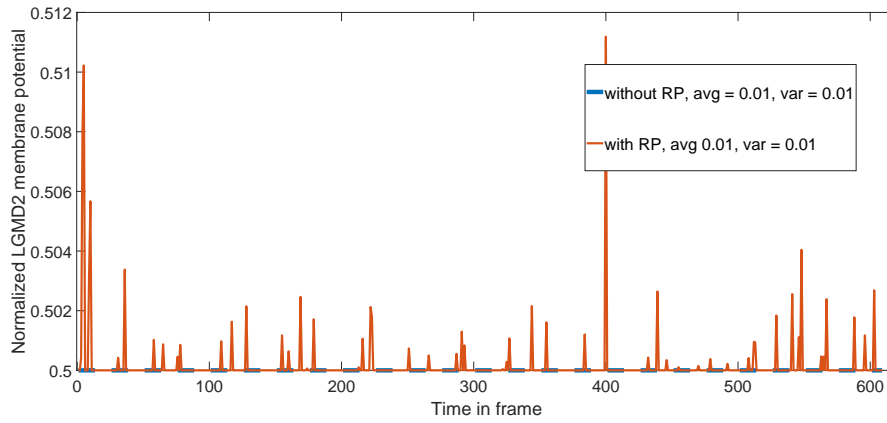


(b) dark translating to the right

Fig. 4.23 For translating motion pattern, LGMD2 shows higher initial membrane potential and more fluctuation against low level Gaussian noise, while completely show contrary results against high level one.



(a)



(b)

Fig. 4.24 (a) At several frames before collision happens (around 399th frame), both model is observed to be mode silenced. When the imminent collision happens, our proposed model shows stronger but not strong enough to generate a spike. (b) Though RP distinguishes itself, the membrane potential remains insufficient for activating LGMD2 neuron to report the collision

Chapter 5

Conclusion and future work

5.1 Conclusion

While cruising in complex real world, locusts amazingly demonstrate their ability to avoid impending collision and incoming objects, such as predators and the homologous of them at high speed. In this thesis, two integrated models for collision perception have been proposed, namely the LGMD1 and LGMD2 with refractoriness mechanism based on prior knowledges of locusts' visual system. By means of mathematically approaching the membrane potential curve, neural refractoriness is simply simulated while space for improvement left. From collected experimental results, the following can be concluded and deduced:

- It is feasible for both LGMD1 and LGMD2 neural network to be endowed with neural refractoriness mechanism. By putting a single layer between retina and medulla, LGMD1 neural network retains its characterization of responding most to looming objects instead of regressing ones. LGMD2 neural network, RP endowed, generates most spikes for dark approaching objects against light background and less for light objects in regressing course, while shows no interests in light approaching objects and dark regressing objects.

- When the approaching objects are at ultra-fast velocity, neural refractoriness improves LGMD1 neural network in terms of accuracy and stability, whilst in a subtle way, helps LGMD2 neural network to retain robustness. It can be apparently observed and derived from statistical test results on LGMD1 model that, neural refractoriness reduces fluctuations evidently when the membrane potential is not high enough to trigger an action potential. Whilst in the manually annotated collision zone, neural refractoriness reduces false positive. For LGMD2 model, neural refractoriness works in only a subtle manner, stabilising the neural output against ultra-fast objects within and outside the annotated collision range.
- When LGMD1 and LGMD2 is encountered with noisy signals, neural refractoriness, to a large extent, makes LGMD1 neuron network stay stable and retain its function, while makes little impacts on LGMD2 network. With noises of higher intensity comes low signal-to-noise ratio. The classic LGMD1 neural cannot work properly even against Gaussian noise of lowest intensity that is tested, whilst work at acceptable success rate against Salt and Pepper noise of lowest intensity. However, performance is worsened with more intensive noise. Neural refractoriness improves its resisting boundary for both two types of noise. Unexpectedly, for LGMD2 model, neural refractoriness fails to impose positive effects on addressing noisy signal problem.

It can be noticed that to different extents, neural refractoriness has demonstrated positive impacts on addressing the two aforementioned real-world challenges, namely ultra-fast approaching objects and noisy signals. LGMD1 neural network for collision perception benefits more from the proposed RP mechanism than the LGMD2, especially the distinguishing test results on noisy signals. Compared with LGMD1, LGMD2 neural networks owns its distinct features and structure, the separated ON/OFF channels and the Photoreceptors Mediation (PM), which complicates its membrane potential calculation and in the mean while enables itself adapt to the cluttered environments. However, since in this thesis numerical simulation

of neural refractoriness is simplified (which is the limitation of this research), it is believed that a more precise mathematical modelling of refractory period should be promising to further improve LGMD2 neural network's robustness and performance to more complex real-world signals.

5.2 Future work

Though our simplified model basically realises characterization of RP mechanism together with the classic LGMD neural networks, compared to modelling RP based on stochastic processes, it remains to be further polished in terms of biological accuracy, especially the relation between maximum and the minimum of the threshold. As shown in Fig. 2.17, the maximum potential is evaluated larger than the absolute minimum potential during the process of hyperpolarization.

The simplified neural refractoriness model is currently tested offline with self-recorded video in the lab on a stationary camera, which strictly speaking does not count for 'cluttered environment'. In future works, the original codes written in Matlab shall be firstly transferring to C++ and then shall be embedded onto micro-mobile platforms such as the aforementioned Colias for further verification on feasibility of real-time calculation and success rate.

In this research, though the whole dataset consists of more than two hundred stimuli clips, number of clips at high-sampling-rate is just around 20, where the background is basically similar. In the exploration of RP's impacts on noisy signals, two types of common noise are used, Gaussian noise and Salt & Pepper noise, which may resemble what our ganglion cells receive at sunset or night, lacking of light. However, it is quite limited, since most of the time locusts flies with sufficient light. Plus, it is because they fly forward instead of hanging in the air that in their field of view, much more objects tend to be moving somehow. Thus, for more precise statistical results, more videos are needed not only in terms of quantity, but also in terms of background difference.

Refractoriness, can be deemed as one of the neuronal spontaneous adaptation to external stimuli. In literatures regarding insects visual systems, another similar mechanism has been noticed, which is called habituation. While refractoriness lasts relatively transitory time usually measured in millisecond, habituation keeps for comparatively longer, and can be observed after several minutes. It is believed that this mechanism assists insects, especially swarm flying insects that usually fly with companies shaking in the field of view, to better filter or get used to stimuli that less matter. Hence, habituation owns its potential for further augmenting LGMD neural networks for collision perception.

References

- [1] Agrawal, S. and Varade, S. W. (2017). Collision detection and avoidance system for vehicle. In *2017 2nd International Conference on Communication and Electronics Systems (ICCES)*, pages 476–477.
- [2] Baek, M., Jeong, D., Choi, D., and Lee, S. (2020). Vehicle trajectory prediction and collision warning via fusion of multisensors and wireless vehicular communications. *Sensors (Basel)*, 20(1):299.
- [3] Bareiss, D., van den Berg, J., and Leang, K. K. (2015). Stochastic automatic collision avoidance for tele-operated unmanned aerial vehicles. In *2015 IEEE/RSJ International Conference on Intelligent Robots and Systems (IROS)*, pages 4818–4825.
- [4] Berry, M. J. and Meister, M. (1998). Refractoriness and neural precision. *Journal of Neuroscience*, 18(6):2200–2211.
- [5] Byrne, J. and Taylor, C. J. (2009). Expansion segmentation for visual collision detection and estimation. In *2009 IEEE International Conference on Robotics and Automation*, pages 875–882.
- [6] Carbone, J., Yabo, A., and Oliva, D. (2018). Characterization and modelling of looming-sensitive neurons in the crab neohelice. *Journal of Comparative Physiology A*, 204:487–503.
- [7] de Vries, S. and Clandinin, T. (2012). Loom-sensitive neurons link computation to action in the drosophila visual system. *Current Biology*, 22(5):353–362.
- [8] Egelhaaf, M., Kern, R., and Lindemann, J. P. (2014). Motion as a source of environmental information: a fresh view on biological motion computation by insect brains. *Frontiers in Neural Circuits*, 8:127.
- [9] Ferrari, U., Deny, S., Marre, O., and Mora, T. (2018). A simple model for low variability in neural spike trains. *Neural Computation*, 30(11):3009–3036.
- [10] Fu, Q., Hu, C., Liu, T., and Yue, S. (2017). Collision selective lgmds neuron models research benefits from a vision-based autonomous micro robot. In *2017 IEEE/RSJ International Conference on Intelligent Robots and Systems (IROS)*, pages 3996–4002.
- [11] Fu, Q., Hu, C., Peng, J., Rind, F. C., and Yue, S. (2020). A robust collision perception visual neural network with specific selectivity to darker objects. *IEEE Transactions on Cybernetics*, 50(12):5074–5088.

- [12] Fu, Q., Wang, H., Hu, C., and Yue, S. (2019). Towards computational models and applications of insect visual system for motion perception: A review. *Artificial Life*, 25(3).
- [13] Fu, Q. and Yue, S. (2015). Modelling lgmd2 visual neuron system. In *2015 IEEE 25th International Workshop on Machine Learning for Signal Processing (MLSP)*, pages 1–6.
- [14] Gabbiani, F. and Dewell, R. B. (2018). Collision avoidance: Broadening the toolkit for directionally selective motion computations. *Current Biology*, 28(3):R124–R126.
- [15] Gabbiani, F., Krapp, H. G., Koch, C., and Laurent, G. (2002). Multiplicative computation in a visual neuron sensitive to looming. *Nature*, 420:320–324.
- [16] Gosiewski, Z., Ciesluk, J., and Ambroziak, L. (2011). Vision-based obstacle avoidance for unmanned aerial vehicles. In *2011 4th International Congress on Image and Signal Processing*, volume 4, pages 2020–2025.
- [17] Halterman, M. W. (2005). Neuroscience, 3rd edition. *Neurology*, 64(4):1–832.
- [18] Hamel, E. and Labib, R. (2019). Modeling biological refractory periods and synaptic depression in an artificial neuron. *Biomedical Physics & Engineering Express*, 5(2):25–38.
- [19] Hampel, D. and Lansky, P. (2008). On the estimation of refractory period. *Journal of neuroscience methods*, 171(2):288–295.
- [20] Hu, C., Arvin, F., and Yue, S. (2014). Development of a bio-inspired vision system for mobile micro-robots. In *4th International Conference on Development and Learning and on Epigenetic Robotics*, pages 81–86.
- [21] Hu, X. L. and Zhang, Y. T. (2000). Effects of refractoriness on the statistics of the post-membrane output ipis. In *Proceedings of the 22nd Annual International Conference of the IEEE Engineering in Medicine and Biology Society (Cat. No.00CH37143)*, volume 1, pages 589–591.
- [22] Li, L., Zhang, Z., and Lu, J. (2021). Artificial fly visual joint perception neural network inspired by multiple-regional collision detection. *Neural Networks*, 135:13–28.
- [23] Nedeveschi, S., Vatavu, A., Oniga, F., and Meinecke, M. M. (2008). Forward collision detection using a stereo vision system. In *2008 4th International Conference on Intelligent Computer Communication and Processing*, pages 115–122.
- [24] O’ Shea, M. and Williams, J. L. (1974). The anatomy and output connection of a locust visual interneurone; the lobular giant movement detector (lgmd) neurone. *Journal of comparative physiology*, 91:257–266.
- [25] Oliva, D. and Tomsic, D. (2014). Computation of object approach by a system of visual motion-sensitive neurons in the crab neohelice. *Journal of Neurophysiology*, 112(6):1477–1490.
- [26] Rind, F. C., Blanchard, M., and Verschure, P. F. M. J. (2000). Collision avoidance in a robot using looming detectors from a locust. In *Sensor Fusion and Decentralized Control in Robotic Systems III*, volume 4196, pages 147–155.

- [27] Rind, F. C. and Bramwell, D. I. (1996). Neural network based on the input organization of an identified neuron signaling impending collision. *Journal of Neurophysiology*, 75(3):967–985.
- [28] Rind, F. C. and Simmons, P. J. (1992). Orthopteran dcmd neuron: a reevaluation of responses to moving objects. i. selective responses to approaching objects. *Journal of Neurophysiology*, 68(5):1654–1666.
- [29] Rind, F. C. and Simmons, P. J. (1999). Seeing what is coming: building collision-sensitive neurones. *Trends in Neurosciences*, 22(5):215–220.
- [30] Rind, F. C., Wernitzing, S., Pölt, P., Zankel, A., Gütl, D., Sztarker, J., and Leitinger, G. (2016). Two identified looming detectors in the locust: ubiquitous lateral connections among their inputs contribute to selective responses to looming objects. *Scientific Reports*, 6(1):35525.
- [31] Ruiz, J. G. (1976). Random threshold element networks with absolute refractory period. *Proceedings of the IEEE*, 64(8):1257–1259.
- [32] Schaette, R., Gollisch, T., and Herz, A. V. M. (2005). Spike-train variability of auditory neurons in vivo: Dynamic responses follow predictions from constant stimuli. *Journal of Neurophysiology*, 93(6):3270–3281.
- [33] Serres, J. R. and Ruffier, F. (2017). Optic flow-based collision-free strategies: From insects to robots. *Arthropod Structure and Development*, 46(5):703–717.
- [34] Simmons, P. J. and Rind, F. C. (1997). Responses to object approach by a wide field visual neurone, the lgmd2 of the locust: Characterization and image cues. *Journal of Comparative Physiology A*, 180:203–214.
- [35] Song, Z., Zhou, Y., and Juusola, M. (2017). Modeling elucidates how refractory period can provide profound nonlinear gain control to graded potential neurons. *Physiological reports*, 5(11).
- [36] Stafford, R., Santer, R. D., and Rind, F. C. (2007). A bio-inspired visual collision detection mechanism for cars: Combining insect inspired neurons to create a robust system. *Biosystems*, 87(2):164–171.
- [37] Sun, H. and Frost, B. J. (1998). Computation of different optical variables of looming objects in pigeon nucleus rotundus neurons. *Nature Neuroscience*, 1(4):296–303.
- [38] Sun, R., Xie, F., Xue, D., Zhang, y., and Ochieng, W. Y. (2017). A novel rear-end collision detection algorithm based on gnss fusion and anfis. *Journal of Advanced Transportation*, 2017.
- [39] Sztarker, J. and Rind, F. C. (2014). A look into the cockpit of the developing locust: looming detectors and predator avoidance. *Developmental neurobiology*, 74(11):1178–1195.
- [40] Sztarker, J. and Rind, F. C. (2014). A look into the cockpit of the developing locust: looming detectors and predator avoidance. *Developmental neurobiology*, 74(11):1078–1095.

- [41] Wang, H., Peng, J., Fu, Q., Wang, H., and Yue, S. (2019). Visual cue integration for small target motion detection in natural cluttered backgrounds. In *2019 International Joint Conference on Neural Networks (IJCNN)*, pages 1–7.
- [42] Wang, H., Peng, J., and Yue, S. (2020). A directionally selective small target motion detecting visual neural network in cluttered backgrounds. *IEEE Transactions on Cybernetics*, 50(4):1541–1555.
- [43] Weis-Fogh, T. and Pringle, J. W. S. (1956). Biology and physics of locust flight ii. flight performance of the desert locust (*Schistocerca gregaria*). *Philosophical Transactions of the Royal Society of London. Series B, Biological Sciences*, 239(667):459–510.
- [44] Yue, S. and Rind, F. (2005). A collision detection system for a mobile robot inspired by the locust visual system. In *Proceedings of the 2005 IEEE International Conference on Robotics and Automation*, pages 3832–3837.
- [45] Yue, S. and Rind, F. C. (2006). Collision detection in complex dynamic scenes using an lgmd-based visual neural network with feature enhancement. *IEEE Transactions on Neural Networks*, 17(3):705–716.
- [46] Yue, S. and Rind, F. C. (2006). Visual motion pattern extraction and fusion for collision detection in complex dynamic scenes. *Computer Vision and Image Understanding*, 104(1):48–60.
- [47] Zhao, J., Hu, C., Zhang, C., Wang, Z., and Yue, S. (2018). A bio-inspired collision detector for small quadcopter. In *2018 International Joint Conference on Neural Networks (IJCNN)*, pages 1–7.
- [48] Zsedrovits, T., Zarandy, A., Vanek, B., Peni, T., Bokor, J., and Roska, T. (2011). Collision avoidance for uav using visual detection. In *2011 IEEE International Symposium of Circuits and Systems (ISCAS)*, pages 2173–2176.

Appendix A

Data sets

Table A.1 Real world video data sets

file name	resolution	frame rate	Approx. velocity
highspeed1	320 x 180	240	5.7143 m/s
highspeed2	320 x 180	240	6 m/s
highspeed3	320 x 180	240	6 m/s
highspeed4	320 x 180	240	6.8571 m/s
highspeed5	320 x 180	240	5.1064 m/s
highspeed6	320 x 180	240	5.2173 m/s
highspeed7	320 x 180	240	6.4865 m/s
highspeed8	320 x 180	240	6.8571 m/s
highspeed9	320 x 180	240	6.1538 m/s
highspeed10	320 x 180	240	6.6667 m/s
highspeed11	320 x 180	240	5.5814 m/s
highspeed12	320 x 180	240	7.7419 m/s
highspeed13	320 x 180	240	8 m/s
highspeed14	320 x 180	240	7.7419 m/s
highspeed15	320 x 180	240	6.6667 m/s
highspeed16	320 x 180	240	6.8571 m/s
highspeed17	320 x 180	240	6.8571 m/s
highspeed18	320 x 180	240	7.2727 m/s
highspeed19	320 x 180	240	9.6 m/s
highspeed20	320 x 180	240	8.5714 m/s
lowspeed1	320 x 180	240	0.8727 m/s

Table A.2 Computer-generated video data sets

file name	resolution	frame rate	description
da	600 x 600	30	A dark square approaching against light background
la	600 x 600	30	A bright square approaching against dark background
dr	600 x 600	30	A dark square regressing against light background
lr	600 x 600	30	A bright square approaching against dark background
de	600 x 600	30	A dark square elongating against light background
le	600 x 600	30	A bright square elongating against dark background
ds	600 x 600	30	A dark square shortening against light background
ls	600 x 600	30	A dark square shortening against dark background
dtl	600 x 600	30	A dark square translating to left side against light background
dtr	600 x 600	30	A dark square translating to right side against light background

Appendix B

Performance Evaluation

Table B.1 Performance evaluation against various Salt and Pepper noise level

Model	Performance	noise density	Approx. SNR
Previous works			
LGMD1	proper	0.001	14.96
LGMD1	failure(boundary)	0.005	8.05
LGMD1	failure	0.01	5.12
LGMD1	failure	0.05	-1.32
LGMD2	okay	0.001	N/A
LGMD2	failure	0.01	N/A
Neural refractoriness endowed			
LGMD1	proper	0.001	14.96
LGMD1	okay	0.005	8.05
LGMD1	failure(boundary)	0.01	5.12
LGMD1	failure	0.05	-1.32
LGMD2	okay	0.001	N/A
LGMD2	failure	0.01	N/A

Table B.2 Performance evaluation against various Gaussian noise level

Model	Performance	noise density	Approx. SNR
Previous works			
LGMD1	failure	0.001	19.96
LGMD1	failure	0.005	12.9
LGMD1	failure	0.01	9.87
LGMD1	failure	0.05	2.9
LGMD2	failure	0.001	N/A
LGMD2	failure	0.01	N/A
Neural refractoriness endowed			
LGMD1	proper	0.001	19.96
LGMD1	failure(boundary)	0.005	12.9
LGMD1	failure	0.01	9.87
LGMD1	failure	0.05	2.9
LGMD2	failure	0.001	N/A
LGMD2	failure	0.01	N/A